
1 **Global simulations of monoterpene-derived peroxy radical fates and the distributions of highly**
2 **oxygenated organic molecules (HOM) and accretion products**

3
4 Ruochong Xu^{1,2,3}, Joel A. Thornton^{1*}, Ben H. Lee¹, Yanxu Zhang², Lyatt Jaeglé¹, Felipe
5 Lopez-Hilfiker^{1,4}, Pekka Rantala⁵, Tuukka Petäjä⁵

6
7 ¹ Department of Atmospheric Sciences, University of Washington, Seattle, WA USA 91895

8 ² School of Atmospheric Sciences, Nanjing University, Nanjing 210023, China

9 ³ Now at Department of Earth System Science, Tsinghua University, Beijing 100084, China

10 ⁴ Now at Tofwerk AG, Thun Switzerland

11 ⁵ Institute for Atmospheric and Earth System Research (INAR) / [Physics](#), University of Helsinki,
12 Helsinki 00014, Finland

13
14 *To whom correspondence should be addressed: joelt@uw.edu

15
16
17 **Abstract**

18 We evaluate monoterpene-derived peroxy radical (MT-RO₂) unimolecular autoxidation and
19 self and cross reactions with other RO₂ in the GEOS-Chem global chemical transport model.
20 Formation of associated highly oxygenated organic molecule (HOM) and accretion products
21 are tracked in competition with other bimolecular reactions. Autoxidation is the dominant
22 fate up to 6-8 km for first-generation MT-RO₂ which can undergo unimolecular H-shifts.
23 Reaction with NO can be a more common fate for H-shift rate constants < 0.1 s⁻¹ or at
24 altitudes higher than 8 km due to the imposed Arrhenius temperature dependence of
25 unimolecular H-shifts. For MT-derived HOM-RO₂, generated by multi-step autoxidation of
26 first-generation MT-RO₂, reaction with other RO₂ is predicted to be the major fate
27 throughout most of the boreal and tropical forested regions, while reaction with NO
28 dominates in temperate and subtropical forests of the Northern Hemisphere. The newly
29 added reactions result in ~4% global average decrease of HO₂ and RO₂ mainly due to faster
30 self-/cross-reactions of MT-RO₂, but the impact upon HO₂/OH/NO_x abundances is only
31 important in the planetary boundary layer (PBL) over portions of tropical forests. ~~Within the~~
32 ~~bounds of formation kinetics and HOM photochemical lifetime constraints from laboratory~~
33 ~~studies, predicted HOM concentrations in MT-rich regions and seasons reach 10% or~~
34 ~~even can~~ exceed total organic aerosol ~~as~~ predicted by the standard version of GEOS-Chem
35 model depending on parameters used. Comparisons to observations reveal large
36 uncertainties remain for key reaction parameters and processes, especially the
37 photochemical lifetime and volatility of HOM, and the rates and branching of associated
38 RO₂-accretion products. ~~Using the highest reported yields and H-shift rate constants of~~
39 ~~MT-RO₂ that undergo autoxidation, HOM concentrations tend to exceed the limited set of~~
40 ~~observations. Similarly, we infer that RO₂-cross reactions rate constants near the gas kinetic~~
41 ~~limit with accretion product branching greater than ~0.25 are inconsistent with total organic~~
42 ~~aerosol unless there is rapid decomposition of accretion products, the accretion products~~
43 ~~have saturation vapor concentrations >> 1 μg m⁻³, or modeled MT emission rates are~~
44 ~~overestimated. This work suggests further observations and laboratory studies related to~~

45 MT-RO₂ derived HOM and gas-phase RO₂-accretion product formation kinetics, and especially
46 their atmospheric fate, such as gas-particle partitioning, multi-phase chemistry, and net SOA
47 formation, are needed.

Formatted: Subscript

48 1. Introduction

49 Monoterpenes are emitted by terrestrial vegetation at a rate of approximately 50 to 100
50 Tg/yr (Arneth et al., 2008; Guenther et al., 2012; Messina et al., 2016), and are a significant
51 component of volatile consumer products (VCP) (McDonald et al., 2018). Reaction of the
52 more common monoterpenes, such as α - and β -pinene, Δ -3 carene, and limonene with
53 atmospheric oxidants is rapid, on the timescale of an hour, and produces a suite of semi-
54 [\(effective saturation concentration, \$C^*\$ is between 0.3 and 300 \$\mu\text{g m}^{-3}\$ \)](#), low ($3 \times 10^{-5} < C^* < 0.3$
55 $\mu\text{g m}^{-3}$), and extremely low ($C^* < 3 \times 10^{-5} \mu\text{g m}^{-3}$) volatility products which contribute to the
56 nucleation and growth of aerosol particles through the formation of secondary organic
57 aerosol (SOA) (Bianchi et al., 2019; Ehn et al., 2014; Hallquist et al., 2009; Kulmala et al.,
58 2014; Palen et al., 1992; Pandis et al., 1992; Zhang et al., 1992). Recent work has shown that
59 even in some isoprene-dominated forested regions, monoterpene oxidation products can be
60 the major component of fine particulate (PM_{2.5}) SOA mass (Lee et al., 2020; Xu et al., 2018;
61 Zhang et al., 2018).

Formatted: Superscript

Formatted: Superscript

Formatted: Superscript

62 Laboratory studies have shown that at least 30 to 50% of the condensable mass produced
63 during oxidation of α -pinene, by both the hydroxyl radical (OH) and ozone, is formed
64 promptly in the first generation of oxidation (Berndt et al., 2016; Ehn et al., 2014; Jokinen
65 et al., 2015; Mentel et al., 2015). This prompt formation of low volatility mass stems from a
66 fraction of the first-generation organic peroxy radicals (RO₂) undergoing repeated
67 unimolecular H-shift reactions followed by O₂ addition, ultimately leading to Highly
68 Oxygenated-organic Molecules (HOM) which are low or even extremely low volatility. The
69 unimolecular H-shifts are the rate-limiting steps to HOM formation, and have been shown
70 for certain RO₂ to exceed 1 s⁻¹ at ~296 K (Xu et al., 2019). At such timescales, bimolecular
71 reactions of RO₂ with the hydroperoxy radical (HO₂), other RO₂, and nitric oxide (NO), even if
72 the latter is present at up to 1 ppb, are not competitive, and autoxidation to HOM is
73 expected to be a dominant fate for such RO₂ in the atmosphere. Moreover, the rate
74 constants of corresponding RO₂ cross-reactions, and the branching to accretion products,
75 presumably organic peroxides (ROOR'), have been shown to be substantially larger than
76 previous expectations (Berndt et al., 2018a, 2018b) and important to new particle formation
77 and growth (Bianchi et al., 2019). The ROOR' products can be of low or extremely low
78 volatility as well, even without substantial RO₂ H-shift chemistry, but cross reactions between
79 isoprene-derived RO₂ and MT-HOM RO₂ specifically can be important in limiting ELVOC
80 formation and thus nucleation ([Öström, et al., 2017](#); [Roldin et al., 2019](#); [McFiggans et al.,](#)
81 [2019](#)).

Field Code Changed

82 Relatively few studies to date have evaluated the global implications of such revisions to our
83 understanding of monoterpene (MT) RO₂ fate (Jokinen et al., 2015; Weber et al., 2020;
84 [Roldin, et al., 2019](#); [Zhu et al., 2019](#)). Jokinen et al. (2015) showed the impact of MT-HOM
85 formation at specified yields on SOA budgets and CCN. Weber et al (2020) use a condensed
86

89 reaction mechanism to more explicitly treat the formation of HOM through unimolecular
90 MT-RO₂ autoxidation and cross reactions, [but, do not conduct global online simulations.](#)
91 [Roldin, et al. 2019 use a similarly explicit mechanism in a 1-D column model to simulate](#)
92 [HOM over a boreal forest setting.](#) [Zhu, et al. \(2019\) do not simulate autoxidation and use a](#)
93 [less stringent definition of HOM than recommended in Bianchi, et al. \(2019\).](#) ~~However, Thus,~~
94 global-scale simulations with online MT-RO₂ chemistry and comparisons to observations,
95 either using total organic aerosol mass as a constraint or more specific molecular
96 composition measurements of gas and aerosol phase species, remain lacking. Moreover, the
97 sensitivity of HO_x, O₃, and NO_x abundances and lifetimes to such changes in RO₂ chemistry
98 have yet to be fully explored in global chemical transport models. The unimolecular MT-RO₂
99 chemistry and faster RO₂ cross reactions have implications for HO_x partitioning, OH recycling,
100 and NO_x lifetime in low-NO_x forested regions. In addition, measurements of highly
101 oxygenated organic nitrates can provide insights into the MT-RO₂ reactivity governing the
102 competitions between autoxidation, RO₂ cross reactions, and RO₂ reactions with nitric oxide
103 (NO).
104

105 Herein, we use the GEOS-Chem global chemical transport model to evaluate the impact of
106 MT-RO₂ H-shift and cross-reactions on tropospheric [Hydrogen-hydrogen](#) oxide radicals (HO_x = OH
107 + HO₂) and total RO₂ abundance, ozone distributions, and assess the potential contribution of
108 MT-HOM and HOM-nitrates to low and extremely low volatility components and by extension the
109 global budget of SOA. We update the GEOS-Chem mechanisms for MT oxidation, using where
110 possible laboratory-derived values of mechanistic parameters, such as MT-RO₂ unimolecular
111 H-shift rate constants, the fraction of MT-RO₂ undergoing H-shifts, and the rate constants for
112 cross-reactions between MT-RO₂ and other RO₂, such as those derived from isoprene oxidation.
113 We compare predicted HOM and HOM-nitrates to atmospheric observations in the gas and
114 particle phases from two locations and conduct sensitivity studies to evaluate the impacts of
115 uncertain kinetic parameters and mechanistic assumptions.
116

117 2. Methods

118 2.1 GEOS-Chem Model

119 We use the GEOS-Chem chemical transport model (Bey et al., 2001) which is driven by
120 assimilated meteorological fields from the MERRA-2 (Modern-Era Retrospective analysis for
121 Research and Applications, Version 2) (Gelaro et al., 2017). Simulations were conducted with
122 2°×2.5° LAT × LON horizontal resolution and 47 vertical levels for 28 months from March
123 2012 to June 2014. This time period provides the best overlap with available observations of
124 monoterpene-derived oxidation products in gas and particle phases made during the SOAS
125 and BAEC field campaigns, described in detail elsewhere (Carlton et al., 2018; Lee et al.,
126 2016, 2018; Lopez-Hilfiker et al., 2016; Petaja et al., 2016), and discussed further below. The
127 first year of the simulation was for spin-up purposes, to allow for accumulation of
128 intermediate chemical reservoir species. For comparison to the observations, we sample the
129 model in time and space corresponding to lowest model grid box containing the location of
130 the observations.
131

132 A reference simulation was conducted based on the public version 12.1.0 of GEOS-Chem

(http://wiki.geos-chem.org/GEOS-Chem_12#12.1.0link). The HO_x-NO_x-VOC-O₃-BrO_x tropospheric chemistry chemical mechanism in the reference simulation is described in Mao et al., (2010, 2013) with recent updates for biogenic VOC chemistry (Fisher et al., 2016; Travis et al., 2016). Emissions of isoprene and monoterpenes are driven by the Model of Emissions of Gases and Aerosols from Nature v2.1 (MEGAN, Guenther et al., 2012). Emissions in GEOS-Chem are based on the Harvard-NASA Emission Component (HEMCO) (Keller et al., 2014). Global anthropogenic emissions of NO_x, SO₂, CO and various aerosol species are from the CEDS (Community Emission Data System) combined with MIX in Asia, NEI in USA, APEI in Canada, BRAVO in Mexico, EMEP in Europe and DICE in Africa. Open fire emissions are from Global Fire Emissions Database (GFED4). Both gas and aerosol are dry-deposited, with rates calculated online based on the resistance-in-series algorithm (Wesely, 1989; Zhang et al., 2001). Wet deposition is calculated for water-soluble aerosol and gas following (Amos et al., 2012; Liu et al., 2001).

2.2 Updates to the GEOS-Chem MT Oxidation Mechanism

Our goal for the mechanism updates was to preserve as much as possible the current simplified framework for MT chemistry in GEOS-Chem, but to include the essential features of MT-RO₂ unimolecular H-shift and bimolecular RO₂ cross-reactions (see Figure 1). Thus, RO₂ and closed-shell products become quickly lumped into corresponding pools that loosely relate to the dominant functional group character, such as carbonyl, alcohol, nitrate, etc. In this version, we restricted changes to chemistry stemming from OH reaction and ozonolysis only, we do not consider nitrate radical (NO₃) reactions of MT. In what follows, to maintain a higher level of clarity, we mostly discuss the mechanism in general terms. Values of mechanistic parameters can be found in Table S1-S5 and are discussed in more detail in the online supplemental information (SI).

To account for MT-RO₂ H-shift chemistry leading to HOM (i.e. "autoxidation"), we split the first-generation MT-RO₂ formed from the reaction of MT with OH or ozone, into two pools, either MT-aRO₂ or MT-bRO₂. Both types of RO₂ undergo the usual bi-molecular reactions, but MT-aRO₂ do not undergo unimolecular H-shift, while MT-bRO₂ do. The branching between MT-aRO₂ or MT-bRO₂ from MT + OH or MT + O₃ reactions are based on laboratory-derived yields of MT-HOM and MT-nitrates, which typically find that the fraction of MT-RO₂ undergoing autoxidation is <0.5 (Berndt et al., 2016; Kurten et al., 2015; Richters et al., 2016) but can be higher in some studies (Xu et al., 2019). The competitive yields of MT-HOM will be sensitive to the multiplicative product of H-shift rate constants and this fraction of first-generation RO₂ able to undergo autoxidation. As a result, we vary this fraction for both OH and O₃ reactions as part of sensitivity studies.

While MT-aRO₂ do not undergo unimolecular H-shifts, we allow for a small fraction (5%) of MT-aRO₂ reactions involving NO or NO₃ to produce MT-bRO₂ to simulate the corresponding alkoxy radicals undergoing opening of the 4-member ring ~~which that~~ is often part of first-generation RO₂ formed from α -pPinene ozonolysis and OH reactions (Kurten et al., 2015; Roldin et al., 2019). This fractional fate of the corresponding alkoxy radical is much lower than assumed by Roldin et al. (2019) and thus our estimates in this regard might produce

177 [lower HOM concentrations. Iyer et al. \(2021\) show that prompt C4 ring-opening from](#)
178 [α-pinene ozonolysis is possible directly from the Criegee bi-radical, and thus reactions with](#)
179 [NO or RO₂ are not necessary for HOM formation. –That said, Opening-opening of the](#)
180 [4-member ring would lead to second-generation RO₂ structures more amenable to](#)
181 [unimolecular H-shift reactions \(Iyer et al., 2021; Kurten et al., 2015\), and provides a means](#)
182 [for enhancing or maintaining HOM formation in the presence of NO as suggested previously](#)
183 [\(Roldin et al. 2019; Pullinen, et al. 2020\), though the balance between alkoxy isomerization](#)
184 [and decomposition remains uncertain.](#)

185
186 [The sequence of autoxidation and base H-shift rate constants used in GEOS-Chem are similar](#)
187 [to those described in Pye et al., 2019 for OH oxidation of MT and Jokinen et al. \(2015\) for MT](#)
188 [+ O₃, which ultimately connect to experimental work in Berndt et al. \(2016\), Jokinen et al.](#)
189 [\(2015\) and Ehn et al., 2014. The mole fraction of first-generation MT-RO₂ able to undergo](#)
190 [unimolecular H-shifts, and thus autoxidation \(MT-bRO₂\), is 20% from MT + OH and 3% from](#)
191 [MT + O₃, in the base simulation \(Table S3\). The HOM mass yield can be 1.5 to 2 times larger](#)
192 [than these molar values. We also note here that GEOS-Chem lumps MT, which can have very](#)
193 [different HOM yields, especially from ozonolysis \(Ehn et al., 2014\). As such, we use the lower](#)
194 [reported HOM yields from ozonolysis of α-pinene to reflect the fact that some of the lumped](#)
195 [MT will be β-pinene or other MT lacking endo-cyclic double bonds. Our range of sensitivity](#)
196 [studies likely capture the associated uncertainty range in these parameters.–](#)

197
198 A single temperature-dependent rate constant, k_{Hshift} , based upon recent laboratory studies
199 and quantum chemical calculation of associated energy barriers is used to describe these
200 H-shifts. We use an activation energy of 17.7 kcal/mol based on the calculations in Berndt et
201 al., (2016). Two values of k_{Hshift} , near 1.0 s⁻¹ and 0.1 s⁻¹ at 298K, are tested in sensitivity
202 studies. The H-shift reactions of MT-bRO₂ are assumed to be followed by O₂ addition to form
203 a new peroxy radical, MT-cRO₂, which in turn can also continue autoxidation to form a yet
204 more oxidized MT-HOM-RO₂. This sequence of RO₂ autoxidation, occurring in competition
205 with typical bimolecular reactions, simulates a first generation of MT-RO₂, C₁₀H₁₅O₄ or
206 C₁₀H₁₇O₃, undergoing two H-shift/O₂ addition steps to form RO₂ with compositions of
207 C₁₀H₁₅O₈ or C₁₀H₁₇O₇, respectively, that are consistent with the current definition of HOM
208 (Bianchi et al., 2019). [We do not track autoxidation of non-C₁₀ RO₂, and thus our definition of](#)
209 [HOM is specific to C₁₀ MT products.](#)

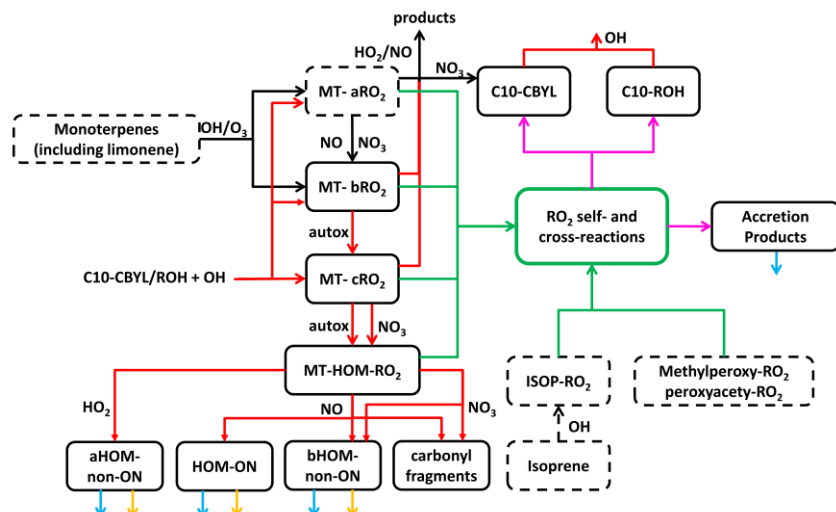
210
211 These MT-HOM-RO₂ undergo only bimolecular reactions with HO₂, RO₂, ~~and~~ NO₂, ~~and~~ NO₃.
212 Except for RO₂ cross-reactions, discussed further below, rate constants for such reactions are
213 the default values used in GEOS-Chem for other RO₂. The products of these reactions are
214 split into four categories, three of which are HOM. Reaction of MT-HOM-RO₂ with HO₂ is
215 assumed to produce only HOM monomers (aHOM) without a nitrate group. Reaction with
216 NO leads to HOM organic nitrates (HOM-ON), a second class of HOM without a nitrate group
217 (bHOM), and hydroxy carbonyl fragments assumed to be C₅ species. The branching ratio for
218 HOM-ON formation is assumed to be 0.2, determined using typical literature
219 parameterizations based on the carbon number. We explicitly distinguish between
220 non-nitrate HOM that result from reaction of MT-HOM-RO₂ with HO₂ (aHOM) or NO (bHOM)

221 to allow for better accounting of RO₂ fate and the specific impact of NO on HOM. The
222 assumption that the alkoxy radical formation channel of MT-HOM-RO₂ reactions with NO
223 leads to HOM is not well constrained, but it is typically a minor component of the HOM yield
224 on a global average. We neglect further autoxidation reactions of RO₂ and alkoxy radicals,
225 and some of the fragmentation channels of the resulting alkoxy radicals may well produce C9
226 or C8 products that still meet the HOM definition. Reaction of MT-HOM-RO₂ with the nitrate
227 radical (NO₃) is assumed to produce only an alkoxy radical product (and NO₂), and the alkoxy
228 radical either forms a bHOM (non-nitrate), similar to that from reaction of the RO₂ with NO,
229 or a C₅ hydroxy carbonyl product to represent fragmentation into non-HOM products. We
230 assume equal branching for these two pathways, which might lead to a slight overestimate
231 of MT-HOM, but reaction with NO₃ is a typically a minor fate for MT-HOM-RO₂.

232
233 After addition of RO₂ H-shift chemistry, the next most significant change to monoterpene
234 chemistry we incorporated into GEOS-Chem involves the self- and cross-reactions of RO₂. We
235 specifically evaluated the impact of a higher rate constant and allowed for accretion product
236 formation in competition to the more common alkoxy radical and disproportionation
237 channels which lead to lumped carbonyl (C10-CBYL) and alcohol (C10-OH) products following
238 the typical lumping strategy in GEOS-Chem. Our basis for these changes includes the recent
239 laboratory studies described in Berndt et al., (2018a, 2018b) and Zhao et al., (2018), where
240 cross-reaction rate constants were found to range from 10⁻¹² to 10⁻¹⁰ cm³ molec⁻¹ s⁻¹ and
241 accretion product branching ranged from 4 to >50%. Given that there are only self-reactions
242 for isoprene-derived RO₂ in the current GEOS-Chem without branching to accretion products,
243 taking even the lower range from laboratory studies would represent a major shift in RO₂
244 fate [as we demonstrate in the results section](#).

245
246 Important for regions with intense biogenic VOC emissions and relatively low NO_x (such as
247 regions of the Amazon), we specifically include cross-reactions between monoterpene and
248 isoprene derived RO₂. Our simulations include both low and high estimates of RO₂ self- and
249 cross-reaction rate constants to better demonstrate the range of possible impacts of these
250 reactions, and we also apply different rate constants for highly oxidized RO₂ (Table S4). For
251 the rate constants considered, RO₂ cross reactions can become competitive or even
252 dominant fates of RO₂ and thus impact the abundance and recycling of HO_x as well as the
253 formation of low volatility products that would contribute to organic aerosol. For accretion
254 products, we use [both](#) a conservative branching (4%) from self- and cross-reactions to
255 produce C20 or C15 compounds, except for HOM-RO₂ self and cross reactions, for which we
256 also examine a [larger ~~unit~~ 100%](#) branching to accretion products as suggested by some
257 laboratory studies (Berndt et al., 2018a, 2018b).

258



259

260 **Figure 1.** The main reactions and processes included in the updated scheme are shown.
 261 Chemical species in solid boxes are newly added while those in dashed boxes already exist in
 262 the GEOS-Chem mechanism. Dashed-line black arrows represent originally existing reactions
 263 without any modification, and solid black arrows represent those with certain modifications
 264 in the scheme. Red, green, and magenta arrows represent newly-added RO₂ formation and
 265 loss. Blue and yellow arrows represent dry-/wet-deposition and photolysis, respectively.
 266 More details are shown in SI.

267

268 We assume the dominant fate of gas-phase MT-HOM as defined here is to partition to
 269 existing aerosol particle mass, and then we assume is dominated by subject to deposition
 270 (wet and dry) or by photolysis in the particle phase. While reaction with OH or other radical
 271 oxidants is possible, our assumption is that the vast majority of HOM produced in this
 272 mechanism will be of low or extremely low volatility and thus be present predominantly in
 273 submicron aerosol particles. Our estimates of HOM mass concentrations are therefore
 274 possibly upper-limits due to the uncertainty in HOM saturation vapor concentrations. As we
 275 do not explicitly consider gas-particle partitioning in this version, we therefore use a single
 276 photolysis frequency equal to 1/60 of j_{NO_2} to account for photochemical degradation of
 277 particle-phase HOM. While we do not treat heterogeneous oxidation explicitly, but we
 278 assume our photolysis parameterization accounts for this process. The value of the
 279 photolysis frequency is based on how well the model reproduces HOM observations in the
 280 absence of further photochemical degradation, and also on laboratory chamber experiments
 281 showing loss of HOM and associated MTSOA mass over time (Krapf et al., 2016; Pospisilova
 282 et al., 2020; Zawadowicz et al., 2020). The photochemical fate of HOM remains one of the
 283 most uncertain aspects of the mechanism.

284

285 We parameterize HOM wet deposition following aerosol-phase organic nitrate in (Fisher et
 286 al., 2016), and dry deposition is calculated online based on the resistance-in-series algorithm

287 (Zhang et al., 2001) assuming HOM behave similarly to SOA (particle dry deposition).
 288 Therefore, the global annually averaged dry deposition velocity of HOM is about 0.06 cm/s
 289 on land. The parameters related to aerosol scavenging, rainout and washout efficiency are
 290 listed in Table S5 following the parameterization of most secondary organic aerosol species in
 291 GEOS-Chem. We note that treating dry deposition of HOM similar to submicron particles is
 292 possibly a small underestimate of the actual HOM dry deposition rate because HOM likely
 293 condense to particles on timescales shorter than those of dry deposition for vapors in most
 294 cases. A typical condensation timescale to aerosol surface area is 15 minutes in the boundary
 295 layer, whereas a deposition velocity of 3 cm s⁻¹ implies a boundary layer average timescale of
 296 several hours. Future updates to the mechanism could consider partitioning of HOM to SOA
 297 based on more explicit tracking of composition-volatility relationships, and thus better
 298 simulate the net depositional scavenging.

299

300 2.3 Simulation Design and Configurations

301 All simulation configurations are summarized in Table 1. A default simulation without HOM
 302 formation nor any other newly-added reactions was run for reference. The base simulation
 303 (LowProd_Photo) was run with relatively conservative MT-bRO2 branching, and with HOM
 304 photolysis turned on, and another simulation with a larger branching ratio to MT-bRO2 was
 305 also run to better determine the HOM formation range (HighProd_Photo). Photolysis of
 306 HOM was also turned off to test its impact in LowProd_noPhoto and HighProd_noPhoto
 307 cases. Another two simulations configured with slow RO₂ self- and cross-reaction rates
 308 (LowProd_Photo_Slow) and slow RO₂ autoxidation rate (LowProd_Photo_kautoSlow)
 309 respectively were used to investigate the sensitivity of HOM and accretion products
 310 formation to these rates. All simulations were conducted in the same way as described in 2.1.
 311 Results were output every month but when comparing with observations, they are output
 312 with 1-hour resolution.

313

314 **Table 1.** Simulations and the corresponding configurations. See text for details.

	MT-bRO2 branching	HOM Photochemical Loss	RO ₂ +RO ₂ rates	kauto 298 K (s ⁻¹)
Default	-	-	-	-
HighProd_noPhoto	high	no	fast	1
HighProd_Photo	high	yes	fast	1
LowProd_noPhoto	low	no	fast	1
LowProd_Photo (base)	low	yes	fast	1
LowProd_Photo_Slow	low	yes	slow	1
LowProd_Photo_kautoSlow	low	yes	fast	0.1

315

316 2.4 Observations

317 Data from three campaigns, the Southern [Ozone-Oxidant](#) and Aerosol Study (SOAS 2013) in
 318 the southeastern United States, the Biogenic Aerosols-Effects on Clouds and Climate (BAECC
 319 2014) in Hyytiälä, Finland and the Green Ocean Amazon Experiment (GoAmazon) in Amazon,
 320 Brazil were used for comparisons (Carlton et al., 2018; Martin et al., 2016; Petaja et al., 2016).

321 Measurements of organic aerosol mass concentrations from aerosol mass spectrometer
322 (AMS) instruments (DeCarlo et al., 2006; Jayne et al., 2000) and gas- and particle-phase HOM
323 from High-Resolution Time of Flight Chemical Ionization Mass Spectrometers (HRTof-CIMS)
324 were used when available (Lopez-Hilfiker et al., 2014). For HOM measurements, molecular
325 formulas of compounds containing 10 carbon atoms and greater than or equal to 7 oxygen
326 atoms were selected as HOM for comparisons. Those with one nitrate ~~atom~~ and without
327 nitrate were compared to simulated HOM-ON and HOM-non-ON, respectively. We also
328 compared predicted HOM to total organic aerosol mass (OA) from aerosol mass
329 spectrometer measurements assuming HOM was present predominantly in submicron
330 aerosol particles. Besides HOM, closely related species in the scheme were also compared
331 when available, including NO, O₃, monoterpenes and isoprene. The details on the
332 measurements were presented in SI including top contributing HOM species identified in
333 data from SENEX and BAECC (Table S7 and S8).

334

335 **3. Results and discussion**

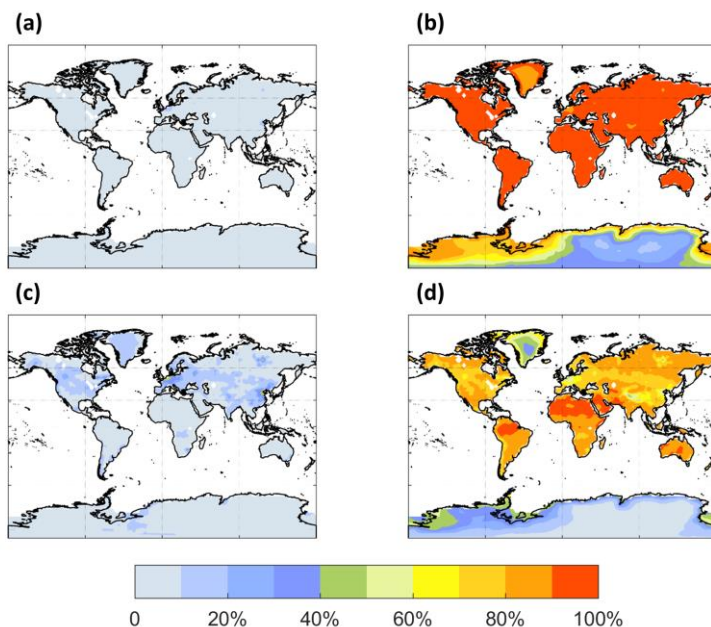
336 **3.1 MT and HOM RO₂ Fates**

337 The largest change to the current mechanism was to the fate of a fraction of MT-derived RO₂,
338 where we incorporated unimolecular autoxidation reactions for a subset of first-generation
339 MT-derived RO₂ (MT-bRO₂ in the above scheme), as well as enhanced reaction rate constants
340 for bimolecular RO₂ self and cross reactions between MT and isoprene RO₂. The fate of RO₂
341 determines the volatility and reactivity of HOM and thus of the potential for HOM
342 contribution to aerosol formation and growth. In our simplified treatment, we assume
343 HOM-RO₂ only undergo bimolecular reactions. HOM-RO₂ that undergo unimolecular
344 decomposition to a closed-shell product, such as by OH or HO₂ elimination, may result in a
345 non-HOM product. Thus, our flux of MT to HOM-RO₂ may be underestimated, but net HOM
346 production may be more accurate.

347

348 The spatial distribution of the annual average reaction fate of MT-bRO₂ in the planetary
349 boundary layer (PBL) is shown in Figure 2 for two simulation cases, LowProd_Photo (panels
350 a-b) and LowProd_Photo_kauto_Slow (panels c-d). The difference between these two
351 simulations is the rate constant for the unimolecular RO₂ H-shift ($\sim 1.0\text{s}^{-1}$ vs. $\sim 0.1\text{s}^{-1}$ at 298K,
352 respectively). For either case, unimolecular H-shift and subsequent autoxidation is the
353 dominant fate of the first-generation MT-bRO₂ throughout the PBL on average. While likely
354 dependent upon model resolution, when k_{auto} is $\sim 0.1\text{s}^{-1}$, the reaction with NO becomes a
355 more common fate for MT-bRO₂, but never more than 50% of the total fate of this HOM-RO₂
356 precursor, even in NO_x-polluted regions such as the SE U.S., eastern China, and Western
357 Europe. In Figure 3, the annually averaged vertical profiles of MT-bRO₂ fate are shown for
358 two model grid points, one containing Centreville, AL and the other in the Amazon
359 containing the T3 site of the Go-Amazon campaign. The dominance of unimolecular RO₂
360 H-shift and autoxidation as a fate for MT-bRO₂ persists up to 6 to 8 km, even though its rate
361 is decreasing exponentially with decreasing temperature. In both locations, reaction with NO
362 at high altitudes becomes a major MT-bRO₂ fate, especially over the SE U.S., while over the
363 Amazon reaction with HO₂ and NO above 6 km are of similar importance likely reflecting the
364 combination of the activation energy required for the unimolecular H-shift, decreases in

365 temperature with altitude, and NO in the upper troposphere from lightning and convection.
 366

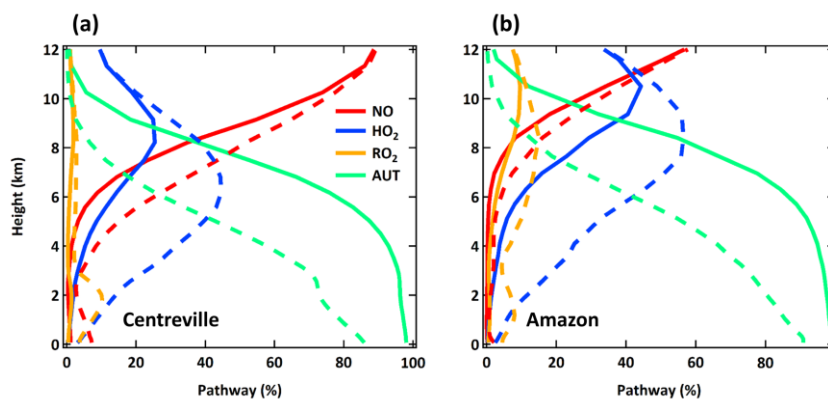


367
 368 **Figure 2.** The annually PBL-averaged MT-bRO₂ consumption fractions by NO (left panel) and
 369 autoxidation (right panel) from experiments LowProd_Photo (a)-(b) and
 370 LowProd_Photo_kauto_Slow (c)-(d). Autoxidation rate constant is $\sim 1.0 \text{ s}^{-1}$ and $\sim 0.1 \text{ s}^{-1}$ at
 371 298K in two experiments, respectively. The fractions by HO₂, NO₃ and RO₂ are shown in
 372 Figure S1.

373
 374 **Table 2.** Global PBL-average MT-bRO₂ fates weighted by gridded MT-bRO₂ concentrations on
 375 land.

		LowProd_Photo	LowProd_Photo_kauto_Slow
MT-bRO ₂	Autoxidation	93%	77%
	NO	1%	6%
	HO ₂	6%	16%
	RO ₂	$\sim 10^{-4}\%$	$\sim 10^{-3}\%$
	NO ₃	0.4%	1.6%

376

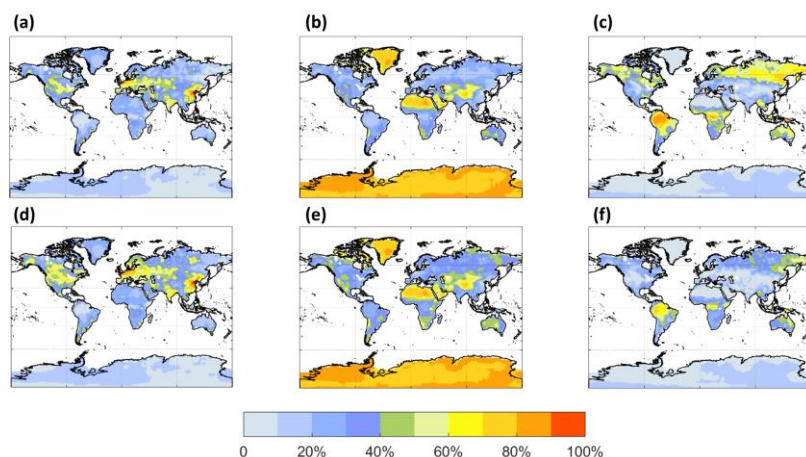


377
 378 **Figure 3.** Annual averaged vertical profiles of four dominant reaction pathways of MT-bRO₂
 379 at Centreville, AL USA and over the Amazon near Manaus, from simulations LowProd_Photo
 380 (solid lines) and LowProd_Photo_kauto_Slow (dashed lines). Reaction with NO₃ contributes
 381 less than 1% and it is thus not shown here.

382
 383 Figures 4 and 5 are similar to Figures 3 and 4, but for the fates of HOM-RO₂ instead of
 384 MT-bRO₂. As HOM-RO₂ in the model do not undergo unimolecular reactions (see above),
 385 these fates are more similar to generic RO₂ chemistry in the model with the important
 386 exception that the rate constants for self and cross-reactions between HOM-RO₂ and other
 387 RO₂ are in general much larger than those typical of other RO₂ in GEOS-Chem. The case
 388 where HOM-RO₂ rate constants for RO₂ cross reactions are relatively large (LowProd_Photo,
 389 Figure 4 panels a-c), e.g. as in Berndt et al., (2018a), reaction with RO₂ is predicted to be the
 390 dominant HOM-RO₂ fate throughout most of the boreal and tropical forest regions as well as
 391 portions of the SE US. In temperate and subtropical forests of the N. Hemisphere, reaction
 392 with NO is the major fate for HOM-RO₂. The potential importance of reactions with RO₂
 393 being a dominant fate is two-fold. First, the branching of such reactions to accretion products
 394 is uncertain (see below), but likely also critical for participation of biogenic VOC in the
 395 nucleation of particles (Bianchi et al., 2019; Kulmala et al., 2014). However, the portion of
 396 such reactions which do not undergo accretion otherwise can result in less carbon mass
 397 moving to lower volatility due to C-C bond scission of alkoxy radical products (Orlando et al.,
 398 2003). In the simulation with slower RO₂ cross-reactions (e.g. LowProd_Photo_Slow), rate
 399 constants for which are near the lower limit of rate constant collections from several
 400 laboratory studies (Berndt et al., 2018a, 2018b; Zhao et al., 2018), RO₂ cross reactions
 401 remain important (~40%) across boreal forests, but are no longer dominant as a HOM-RO₂
 402 fate except in the tropical forest regions. Reactions with NO expand in importance in boreal
 403 forest regions in this simulation, at times being the dominant fate in regions of the N.
 404 American boreal forest. While consistently significant, typically at 30 to 40% of HOM-RO₂ fate,
 405 reaction of HOM-RO₂ with HO₂ is only rarely a majority fate in the PBL over forested regions.

406
 407 The annual average HOM-RO₂ fate changes significantly between the boundary layer and
 408 free troposphere as shown in Figure 5 for the same two model locations in Figure 3.

409 Throughout the low and middle troposphere in both locations, reaction with HO₂ becomes
 410 the dominant HOM-RO₂ fate in both locations, followed by RO₂ over the Amazon, and NO
 411 over the SE US. Reaction with NO becomes the dominant fate for HOM-RO₂ in the upper
 412 troposphere over the SE US, while NO, HO₂ and RO₂ reactions are predicted to be of similar
 413 importance over the Amazon.

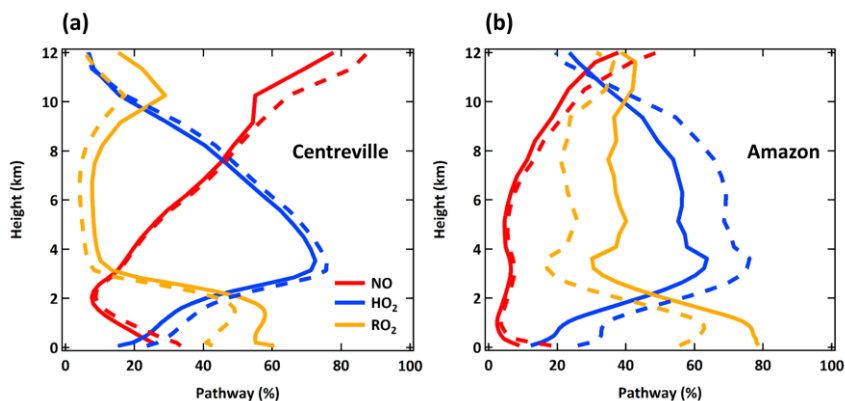


414
 415 **Figure 4.** The annually PBL-averaged MT-HOM-RO₂ relative fates including reaction with NO
 416 (left panel), HO₂ (middle panel) and RO₂ (right panel) from simulation LowProd_Photo (a)-(c)
 417 and LowProd_Photo_Slow (d)-(f). Reaction with NO₃ contributes <1% and it is thus not
 418 shown here.

419
 420 **Table 3.** Global PBL-average MT-HOM-RO₂ fates weighted by gridded MT-HOM-RO₂
 421 concentrations on land.

		LowProd_Photo	LowProd_Photo_Slow
MT-HOM-RO ₂	NO	16.44%	20.71%
	HO ₂	22.00%	33.12%
	RO ₂	61.54%	46.11%
	NO ₃	0.02%	0.06%

422



423

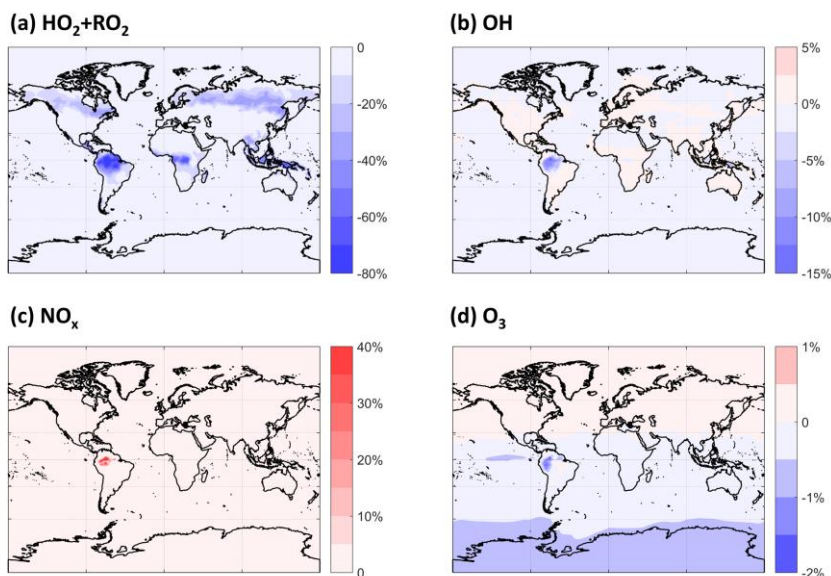
424 **Figure 5.** Annual averaged vertical profiles of three dominant reaction pathways of
 425 MT-HOM-RO₂ at Centreville, AL and Amazon near Manaus, from simulation LowProd_Photo
 426 (solid lines) and LowProd_Photo_Slow (dashed lines). Reaction with NO₃ contributes < 1%
 427 and it is thus not shown here.

428

429 3.2 Impact on HO_x, NO_x, and O₃

430 By altering the fates of MT-derived RO₂ chemistry and the interactions thereof with
 431 isoprene-derived RO₂, we expect that the cycling and lifetime of HO_x are affected. Changes in
 432 HO_x abundance and distribution will alter NO_x cycling and fate, which will potentially impact
 433 tropospheric O₃. MT are not typically major components of OH reactivity, even in
 434 biogenically influenced regions so these impacts are not expected to be large. As shown in
 435 Figure 6, there are substantial decreases in the sum of HO₂ and RO₂ concentrations in certain
 436 regions averaged over the planetary boundary layer (PBL), the height of which is taken from
 437 the MERRA-2 reanalysis data (Gelaro et al., 2017). HO₂ and RO₂ concentrations together
 438 decrease by as much as ~20% over boreal forests and up to 80% over tropical forests. The
 439 global average decrease in the sum of HO₂ and RO₂ in this simulation compared to the
 440 default is 4%. The updated description of RO₂ self and cross reactions is the dominant driver
 441 of the shorter RO₂ lifetime and thus of the calculated decreases. Given that most of these
 442 decreases in RO₂ occur in locations with low NO, the impact upon HO₂ and OH (Figure 6b) are
 443 small globally, but not negligible in the PBL over the Amazon, reaching a ~15% decrease in
 444 OH. The lower OH predicted over the Amazon leads to longer NO_x lifetimes there and thus a
 445 highly localized increase in NO_x abundance. Otherwise, the effects on NO_x and O₃ are
 446 negligible globally.

447



448
 449 **Figure 6.** The annual PBL-averaged relative differences of (a) HO₂+RO₂, (b) OH, (c) NO_x and (d)
 450 O₃ between simulations LowProd_Photo and Default.

451
 452
 453
 454

4553.3 HOM and associated accretion product distribution and concentrations

456 **Table 4.** Global annual budgets of MT-HOM and MT-RO₂ accretion products
 457 from Mar. 2013 to Feb. 2014 (unit: kt C).

	Chemistry	Wet deposition	Dry deposition
HOM-non-ON	321	-277	-45
HOM-ON	26	-20	-6
Total accretion products	2107	-1907	-204

458
 459 Global annual budgets for the chemistry (Production + Loss), and wet and dry deposition of
 460 HOM-non-ON, HOM-ON and MT-derived accretion products are summarized in Table 4 from
 461 the LowProd_Photo_kauto_slow simulations. For even the slowest kauto used, the
 462 non-nitrate pathway for HOM is more than factor of 10 that of HOM organic nitrates.
 463 Interestingly, even for a small branching to accretion products, MT-RO₂ derived accretion
 464 products are a substantially larger fate than HOM, suggesting either that the rates and
 465 branching are too high or that the chemical loss pathways of associated products are not
 466 well represented.

467
 468 The PBL average mass concentrations (μg m⁻³) of HOM predicted by the model are shown in

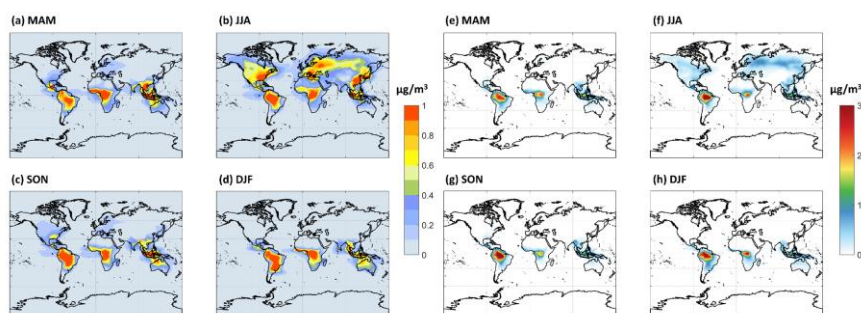
469 Figure 7 (a-d) for the LowProd_noPhoto, which produces middle-to-upper range estimates of
470 HOM concentrations out of the other scenarios tested. Maps from other sensitivity
471 simulations are included in the SI (Figure S2-S6). In this scenario, monoterpene-derived HOM
472 are predicted to average near $1 \mu\text{g m}^{-3}$ in the PBL over tropical forests with little seasonality,
473 while in the temperate and boreal forests of N. America, Europe, and east Asia, HOM reach
474 0.5 to $1 \mu\text{g m}^{-3}$ during summer months. In the LowProd_Photo scenarios, HOM
475 concentrations average an order of magnitude lower than shown in Figure 7, though the
476 spatial and seasonal patterns are similar. Given that HOM with 10 carbons and 7 or more
477 oxygens will be low or extremely low volatility, the majority of HOM produced from
478 monoterpene oxidation will likely contribute to SOA and thus to total OA. A background
479 organic aerosol mass concentrations in rural or remote forested regions of order $1 \mu\text{g m}^{-3}$
480 outside of biomass burning periods is not atypical (Jimenez et al., 2009).

481
482 For comparison, we also show seasonal PBL distributions of HOM-RO₂ self or cross reaction
483 accretion products, assuming the C₂₀-HOM are formed at unit yield. This assumption
484 provides an upper-limit, but one which is supported by some laboratory studies (Berndt et
485 al., 2018a and b). Throughout the tropical forests and boreal regions during summer,
486 HOM-RO₂ accretion products in this simulation reach 3 or $1 \mu\text{g m}^{-3}$, respectively. As total OA
487 in some boreal and tropical forest measurements can be on this order (Jimenez et al., 2009;
488 Lee et al., 2018; de Sa et al., 2018) outside of biomass burning periods, we conclude
489 C₂₀-HOM undergo particle phase decomposition and/or the HOM-RO₂ self and cross
490 reactions do not produce accretion products at unit yield or the model underestimates NO
491 throughout boreal and tropical forest regions which would suppress both HOM and more so
492 HOM accretion product concentrations. As shown in the SI (Figure S7), assuming an accretion
493 product branching of 4% for all MT-RO₂ self or cross reactions, as in Zhao, et al. (2019),
494 including HOM-RO₂, leads to significantly lower, but not unimportant, concentrations of
495 accretion products. The total C₁₅ + C₂₀ accretion product concentrations in the PBL of tropical
496 and boreal forest regions are typically less than 1 or $0.25 \mu\text{g m}^{-3}$, respectively, in this
497 simulation.

498
499 Accretion products from HOM-RO₂ reactions with other HOM-RO₂ are likely an important
500 route to new particle formation especially in the relatively warm planetary boundary layer.
501 Thus, to predict new particle formation in regions such as the remote temperate or boreal
502 forests, such accretion products will need to be incorporated. As noted above, the self and
503 cross reaction rates and accretion product branching in both cases are far larger than those
504 commonly used in GEOS-Chem. Nucleation and growth of particles by MT-HOM and
505 associated accretion products is beyond the scope here, but in both treatments of accretion
506 product formation, C₂₀ HOM accretion products reach concentrations which are likely
507 relevant for participation in new particle formation (e.g. 10^7 - 10^8 molec cm⁻³) to the extent it
508 occurs in the PBL over forested regions (Bianchi et al., 2019). A remaining question is to what
509 extent MT-RO₂ derived accretion products more generally form and contribute to OA mass.

510
511 Our results suggest that further refinement of HOM formation and loss kinetics is needed
512 since the range of our simulations suggest HOM either make relatively small contributions to

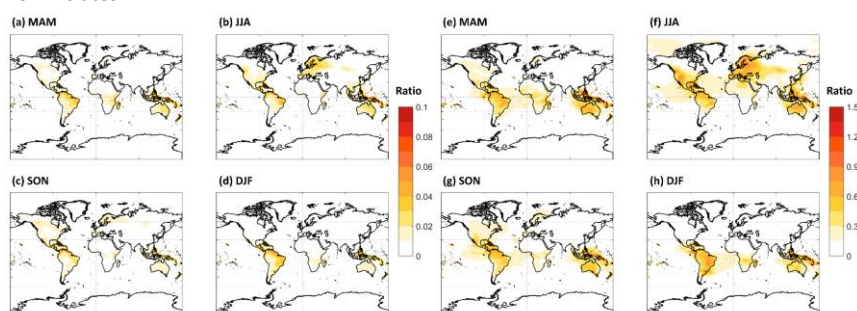
513 regional OA or constitute the majority of OA outside of biomass burning periods over
514 tropical forests year-round, and during summer months for temperate and boreal forests.
515 Figure 8 illustrates that for two of the sensitivity simulations which bound possible HOM
516 formation and loss kinetics, MT-HOM concentrations alone are either 5 to 10% of total OA
517 predicted by the standard GEOS-Chem model or are more than a factor of 1.5 higher than
518 the predicted total OA. Incorporating predicted MT-RO₂ derived C₁₅ and C₂₀ accretion
519 products as an OA source only increases the potential contribution of MT to total OA. If the
520 MT-RO₂ accretion product branching is on average 4%, accretion products can double the
521 contribution of MT to OA when HOM are simulated in the LowProd_Photo case (see Figure
522 S7). If the accretion branching ratio is closer to unity, as expected for HOM-RO₂, the
523 contribution of HOM monomers and MT-HOM accretion products to OA is even larger,
524 reaching or exceeding a mean ratio of 3 in tropical forests compared to GEOS-Chem
525 predicted OA. Thus, revising MT chemistry to incorporate gas-phase sources of low and
526 extremely low volatility pathways will likely increase, perhaps substantially, the total OA
527 predicted by the GEOS-Chem model over forested regions.
528



529
530 **Figure 7.** The seasonal PBL-averaged total HOM mass concentrations of (a) MAM, (b) JJA (c)
531 SON and (d) DJF from experiment LowProd_noPhoto. Seasonal PBL-averaged total C₂₀ HOM
532 accretion products are shown in panels e-h, assuming HOM-RO₂ self and cross reactions
533 produce accretion products at unit yield.
534

535 There are limited observations of HOM that can be used to investigate the validity of the
536 different scenarios simulated here. First, the majority of HOM will condense to form SOA,
537 where they may further react to form products that might not be traceable to HOM formed
538 in the gas-phase (Krapf et al., 2016; Lee et al., 2020; Pospisilova et al., 2020; Zawadowicz et
539 al., 2020). Second, most HOM have been observed only in the gas-phase (Bianchi et al., 2016;
540 Ehn et al., 2014; Massoli et al., 2018), which represents only a local steady-state between the
541 formation and condensation sink over small spatial scales compared to the current model
542 resolution. The FIGAERO HRToF-CIMS instrument measures some HOM in both the gas and
543 particle phases, while the aerosol mass spectrometer (AMS) provides an upper limit
544 constraint on the total organic aerosol. In Figure 8, we show observations from the FIGAERO
545 HRToF-CIMS at a rural temperate and rural boreal forest, in Centreville, AL in the Southeast
546 U.S. and SMEAR II station in Hyytiälä, Finland, respectively, [using only C₁₀ compounds](#). In

547 addition, we show AMS observations of total OA from these sites as well as from the T3 site
548 of the Go-Amazon campaign outside of Manaus, Brazil. The Centreville, AL observations were
549 obtained in June-July 2013, the SMEAR II observations were from April –June 2014, and the
550 Go-Amazon observations were from February-March 2014. More information can be found
551 in SI and related papers (Carlton et al., 2018; Martin et al., 2016; Petaja et al., 2016). The
552 FIGAERO HRTof-CIMS observations include both speciated HOM organic nitrates and
553 non-nitrates.



554 **Figure 8.** The seasonal PBL-averaged total C₁₀-HOM mass concentrations from the
555 LowProd_Photo (a-d) or the HighProd_noPhoto (e-h) simulations plotted relative to the total
556 OA mass concentration predicted by GEOS-Chem for the same periods and locations. Note
557 the color scale for panels a-d (0 to 0.1) is about a factor of 10 lower than that for panels e-h
558 (0 to 1.5).
559

560 We compare these observations to two simulations, HighProd_Photo and LowProd_Photo,
561 where each includes photochemical losses of HOM based on recent experimental work
562 (Zawadowicz et al., 2020), but different yields of MT-bRO₂ that can undergo unimolecular
563 H-shifts as discussed above. The comparison is challenged for a number of reasons. First,
564 monoterpene emissions are uncertain in a global sense but will also vary significantly at
565 scales below the resolution of the model. Second, gas-phase HOM will be sensitive to the
566 local oxidant conditions, [which will also depend on model predicted NO concentrations and](#)
567 [BVOC](#), while particulate HOM potentially represent the integral of multiple days of formation,
568 loss, and transport. Moreover, HOM in the particle phase may react into non-HOM, be lost
569 on instrument surfaces, or thermally decompose during the analysis, such that observations
570 of total HOM are possibly underestimated by the FIGAERO HRTof-CIMS instrument. To
571 facilitate the comparison, we use the diurnal cycle in observations averaged over 4 to 6
572 weeks of observations to minimize the impact of meteorological variability. [Addressing errors](#)
573 [in the MEGAN emissions inventory is beyond the scope of this paper, therefore, We-we scale](#)
574 [the predicted HOM concentrations in the lowest model level by the ratio of observed to](#)
575 [predicted monoterpene concentrations in order to account for potential biases in the](#)
576 [regional monoterpene emissions in the model](#) (Figure S8). For SOAS and GoAmazon, we use
577 the hourly average measured monoterpene data to compare with the hourly GEOS-Chem
578 predictions, while for the BAEEC campaign at SMEAR II station, we use the campaign average
579 of measured monoterpene concentrations. We separate HOM organic nitrates (ON) from
580 HOM non-nitrates (non-ON) where possible but compare to the total measured gas + particle
581

582 in each category.

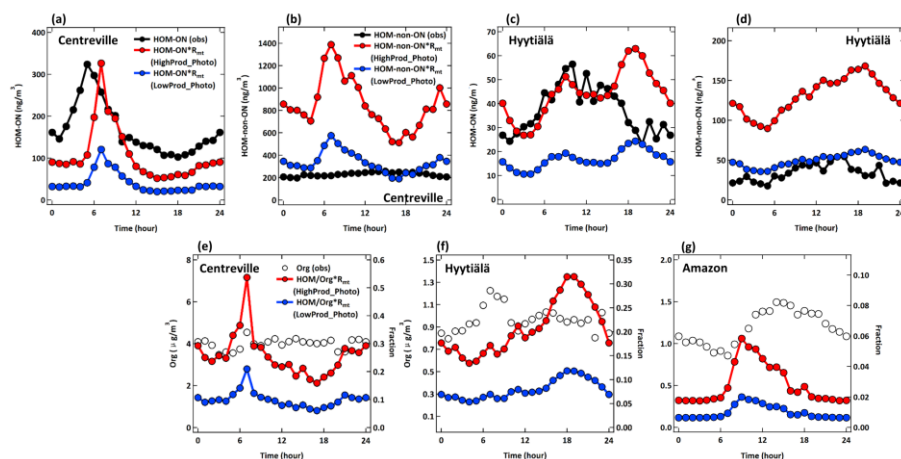
583

584 As shown in Figure 9, there is general order-of-magnitude agreement between the observed
585 HOM and those predicted by one of the model simulations when adjusted by the predicted
586 and observed monoterpene concentrations as described above. The HighProd_Photo
587 simulation is better able to simulate the HOM-ON, but overestimates the non-ON HOM
588 measured in the boreal forest location. In contrast, in the Centreville location, the
589 HighProd_Photo simulation underestimates the measured HOM-ON but overestimates the
590 measured non-ON HOM. The general overestimation of observed non-ON HOM could be due
591 to the non-ON HOM having reacted in the particle phase into components that are not
592 detectable as HOM due to analytical limitations of the instrument used, which relies on
593 thermal desorption and thus can be subject to thermal decomposition of low volatility
594 components [Lopez-Hilfiker et al., 2014]. We note that the HighProd_Photo simulation does
595 not overestimate the observed fine mode OA mass concentrations in any of the three
596 locations, such that there is potential for a higher fraction of MT oxidation to result in HOM
597 and higher contributions of MT-HOM to OA than shown in Figure 9. The reason for a low
598 contribution of MT-HOM to OA predicted for the Amazon region remains unknown, but
599 possibly related to errors in the modeled MT emission inventory, limitations of comparing a
600 relatively coarse model resolution to a single location measurement, and/or the influences
601 from isoprene, biomass burning, and other pathways are perhaps more important in this
602 location.

603

604 The general shape of the HOM diurnal cycle and HOM relative to OA (Figure 9) are typically
605 well captured for each location, except for the late evening and early morning periods
606 possibly due to issues simulating the nocturnal layer relative to the emission height of
607 monoterpenes. In the Amazon location, there is a clear late afternoon peak in the measured
608 OA that is not present in the predicted monoterpene derived HOM concentrations. These
609 comparisons suggest that based on the current set of observations we cannot conclude
610 which set of HOM formation and loss kinetics is most appropriate for describing ambient
611 HOM. We can conclude that total HOM abundances, including both ON and non-ON HOM,
612 are potentially higher than those shown in Figure 9, similar to those predicted by the
613 HighProd_Photo case or the LowProd_noPhoto case, with PBL average mass concentrations
614 in monoterpene rich regions and seasons of order 0.5 to 1 $\mu\text{g m}^{-3}$, see, e.g., Figures S9 and
615 S10. Uncertainties in first-generation RO_2 branching parameters, isomerization rate constants,
616 and HOM chemical fate remain large, with limited observational constraints on total HOM
617 concentrations (gas + particle).

618



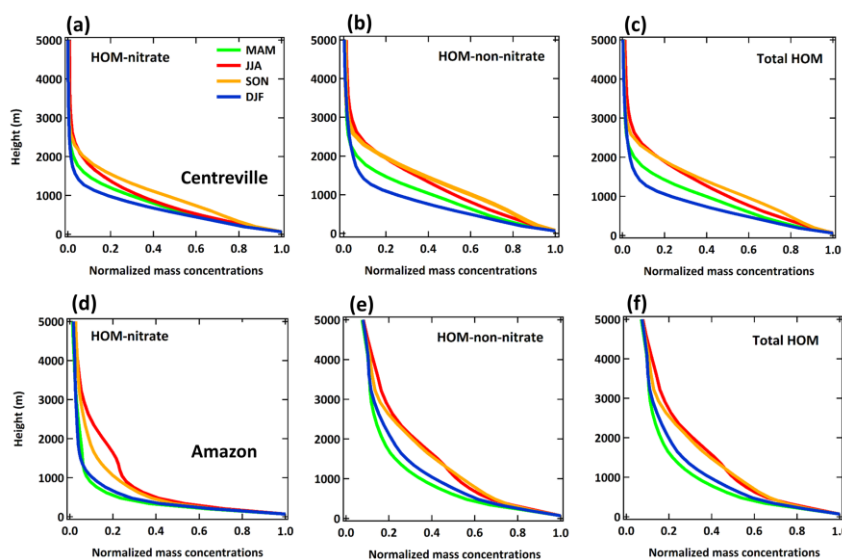
619
 620 **Figure 9.** Diurnal changes of observed (black line) and simulated (HighProd_Photo: red line;
 621 LowProd_Photo: blue line) (a) HOM-ON and (b) HOM-non-ON mass concentrations at
 622 Centreville site. (c)-(d) The same as (a)-(b) but at Hyttiälä site. (e)-(f) Diurnal changes of
 623 observed organic aerosol mass concentrations (black hollow circle markers) and the fractions
 624 that simulated total HOM account for of observed organic aerosols (HighProd_Photo: red;
 625 LowProd_Photo: blue) at Centreville, Hyttiälä and Amazon sites, respectively.

626
 627 **3.4 Vertical profiles of HOM**

628 Figure 10 summarizes the vertical distribution of HOM predicted by the LowProd_Photo
 629 simulation for two locations, one over the SE US SOAS site and one over the Amazon region
 630 using the same grid which contains the GoAmazon T3 site (Martin et al., 2016). Evident is the
 631 expected predominance of monoterpene present within the PBL in all seasons and locations
 632 related to the surface vegetation source. Also evident is the different vertical profiles of
 633 HOM-ON compared to non-ON HOM, with slower decays with altitude of non-ON HOM up to
 634 2 to 3 km above the surface during JJA in both the SEUS and Amazon regions, likely due to
 635 changes in the HOM-RO₂ fate with altitude (see 3.1). Over the Amazon during JJA and SON,
 636 both non-ON HOM and HOM-ON concentrations are predicted to be relatively enhanced
 637 between 1 to 5 km compared to the lowest altitude concentrations. The relative
 638 enhancement in this altitude region during JJA and SON compared to DJF and MAM likely
 639 reflects overall drier conditions but also significant vertical transport of HOM precursors
 640 during these seasons, e.g. through shallow convection. The relative enhancements
 641 specifically between 1 to 4 km compared to altitudes higher than 5km could also reflect the
 642 temperature dependence of the unimolecular H-shift rate constant describing monoterpene
 643 derived RO₂ autoxidation and changing bimolecular reaction rates with altitude. This
 644 relative enhancement is not as obvious in the vertical profiles over the SEUS, which appear
 645 as smoother monotonic decays with altitude, and that are higher in abundance during
 646 summer months.

647
 648 HOM-RO₂ accretion products illustrate similar vertical profiles as the HOM monomers (see SI

649 Figures S12 and S13). If we use the rate constants reported by Berndt et al., (2018a, 2018b)
 650 together with branching ratio of unity for HOM-RO₂ derived accretion products, the seasonal
 651 mean abundance of predicted total of C₁₅ and C₂₀ HOM accretion products reaches 1 to 5 μg
 652 m⁻³ in the PBL over the SE US and tropical forested regions respectively (see SI), and decay to
 653 1x10⁻³ and 3x10⁻² μg m⁻³ (1x10⁶ and 4x10⁷ molec cm⁻³), respectively, in the upper troposphere
 654 over these regions. Assuming instead a HOM-RO₂ accretion product yield of 4%, the
 655 predicted total of C₁₅ and C₂₀ HOM accretion products are between 0.2 and 1 μg m⁻³ over the
 656 SE US and tropical forests, respectively, decaying to 2x10⁻⁴ and 7x10⁻³ μg m⁻³ (3x10⁵ and 1x10⁷
 657 molec cm⁻³) in the upper troposphere. At such *average* concentrations in the upper
 658 troposphere over these regions, we conclude either type of HOM accretion product will
 659 likely contribute significantly to new particle formation and growth, but uncertainty in the
 660 accretion product branching of HOM-RO₂ reactions would lead to a factor of 4 or more in the
 661 estimated contribution.
 662



663
 664 **Figure 10.** The seasonal averaged vertical profiles of HOM-ON (left panel), HOM-non-ON
 665 (middle panel) and total HOM (right panel) at Centreville (top panel) and Amazon (bottom
 666 panel). All the results are from experiment LowProd_Photo. Values are normalized to the
 667 lowest-level values of each season. The profiles with absolute concentrations are shown in
 668 Figure S9.
 669

670 4. Conclusion

671 We implemented a new mechanism to describe MT-derived RO₂ chemistry in the
 672 GEOS-Chem global chemical transport model. The mechanism is relatively simple, adding 10
 673 species and 37 reactions to the standard mechanism, without substantial addition of
 674 computation time. We focused on updating the representation of unimolecular H-shift
 675 reactions to form HOM-RO₂ and their fate, as well as the self- and cross-reactions of

676 MT-derived RO₂ and isoprene derived RO₂. Several sensitivity studies were conducted to
677 evaluate the impact of various mechanism parameters and associated uncertainties, and
678 where possible we compared to observations. The results from these sensitivity studies show
679 that for a model resolution of 2° x 2.5°, uncertainty in the average H-shift rate constant is less
680 important for predicted HOM concentrations than the fraction of MT reactions with OH or O₃
681 to form RO₂ which can undergo H-shift and autoxidation and the photochemical lifetime of
682 HOM. While a comprehensive comparison of HOM predictions to OA remains, in three
683 locations, the model predictions of HOM did not exceed total measured OA mass
684 concentrations, which is currently the strongest constraint on HOM. However, using
685 HOM-ON measurements as a guide suggests that if the fraction of MT-RO₂ that undergo
686 relatively rapid H-shift ($k_{\text{auto}} > 0.1 \text{ s}^{-1}$) is greater than 0.25, then significant photochemical
687 losses of HOM mass from particles that is faster than wet or dry deposition of particulate
688 organics is required. Indeed, the current estimates of MT-derived HOM monomer and HOM
689 accretion product formation rates from laboratory studies lead to mass concentrations of the
690 same order as or event OA mass concentrations predicted by the model. However,
691 uncertainties in emission inventories of BVOC and small absolute errors in NO or NO₂
692 concentration fields in global scale models contribute additional uncertainty into the most
693 appropriate set of parameters to use. Additional refinement of the branching to MT-RO₂
694 which can undergo H shifts and mechanistic insights into HOM photochemical lifetime are
695 clearly needed. That The current estimates of MT derived HOM monomer and HOM
696 accretion product formation rates from laboratory studies lead to mass concentrations of the
697 same order as OA mass concentrations predicted by the model, indicating that a
698 comprehensive online coupling of this updated MT-RO₂ chemistry to aerosol formation in
699 GEOS-Chem and other models is needed.

Formatted: Subscript

700
701 The majority of HOM production occurs in the continental boundary layer where MT
702 emissions are significant, including boreal, temperate and tropical regions. H-shift and
703 autoxidation is the major fate for the subset of MT-RO₂ with that capability, outcompeting
704 reactions with NO, HO₂ and RO₂ up to 6 km altitude in relatively unpolluted regions.
705 Autoxidation of first-generation MT-RO₂ is significantly slower in the upper troposphere and
706 likely uncompetitive with reactions with NO and HO₂. As such, HOM formation in the outflow
707 of deep convection is unlikely, though HOM formation from MT detraining from shallow
708 convection below 6 km is feasible.

709
710 Implementing faster self and cross-reactions between RO₂ in GEOS-Chem as found by Zhao et
711 al. (2019) and Berndt et al. (2018a) lead to significantly lower HO₂ and RO₂ concentrations in
712 boreal and tropical forested regions (by 20% or more compared to the standard mechanism), but
713 globally average changes in OH, NO_x, and O₃ are negligible. These reactions also alter the fate of
714 MT-RO₂, especially MT-derived HOM-RO₂, for which reaction with MT-derived and other RO₂
715 (typically isoprene-derived) is the dominant fate throughout the boundary layer neglecting
716 unimolecular HOM-RO₂ reactions. While perhaps unexpected compared to previous RO₂ fate
717 assessments using slower RO₂ self and cross reaction rate constants, such such a situation can be
718 supported in part by the molecular composition measurements of MT-HOM which show
719 significant contributions of HOM with H numbers less than 16 and odd-numbers of O, e.g.,

720 C₁₀H₁₄O₉. This evidence alone is not sufficient, as HOM-RO₂ reactions with NO could also produce
721 similar results. [Future field campaigns that constrain the relevant NO_x and oxidant fields together](#)
722 [with HOM in low-NO_x regions could provide important constraints in this regard.](#)

723
724 ~~Moreover,~~ The branching to accretion products [of RO₂ self and cross reactions](#) is a key parameter
725 with significantly different ranges produced by laboratory studies. The concentrations of C₁₅ and
726 C₂₀ accretion products predicted using self and cross-reaction rate constants of ~10⁻¹¹-10⁻¹⁰ cm³
727 molec⁻¹ s⁻¹ with a conservative branching (4%) from Zhao et al (2018), are typically small
728 compared to average OA mass concentrations, except in the tropical forested regions, where
729 these accretion products alone are likely similar to background OA concentrations outside of
730 biomass burning events. Using a larger branching to accretion products as supported by studies
731 by Berndt et al (2018) leads to such accretion products likely dominating low volatility products
732 that could contribute to OA, with predicted mass concentrations well exceeding OA mass
733 concentrations in remote tropical regions. Thus, further refinement in the rate constants and
734 branching to gas-phase accretion products and their photochemical fates are needed, especially
735 since these products from HOM-RO₂ cross reactions are likely essential in the contributions of MT
736 to new particle formation (Bianchi et al., 2019; McFiggans et al., 2019) especially over tropical
737 forested regions (Andreae et al., 2018; Wang et al., 2016; Zhao et al., 2020).

738 739 **Acknowledgements**

740 JAT was supported by a grant from the National Science Foundation (CHE-1807204) and the U.S.
741 Department of Energy Atmospheric Science Research program (DE-SC0021097). RX thanks
742 Nanjing University for an undergraduate research fellowship.

743 744 **References Cited**

745 Amos, H. M., Jacob, D. J., Holmes, C. D., Fisher, J. A., Wang, Q., Yantosca, R. M., Corbitt, E. S.,
746 Galarneau, E., Rutter, A. P., Gustin, M. S., Steffen, A., Schauer, J. J., Graydon, J. A., St Louis, V.
747 L., Talbot, R. W., Edgerton, E. S., Zhang, Y. and Sunderland, E. M.: Gas-particle partitioning of
748 atmospheric Hg(II) and its effect on global mercury deposition, *Atmos. Chem. Phys.*, 12(1),
749 591–603, doi:10.5194/acp-12-591-2012, 2012.

750 Andreae, M. O., Afchine, A., Albrecht, R., Holanda, B. A., Artaxo, P., Barbosa, H. M. J., Borrmann,
751 S., Cecchini, M. A., Costa, A., Dollner, M., Fuetterer, D., Jaervinen, E., Jurkat, T., Klimach, T.,
752 Konemann, T., Knote, C., Kraemer, M., Krisna, T., Machado, L. A. T., Mertes, S., Minikin, A.,
753 Poehlker, C., Poehlker, M. L., Poeschl, U., Rosenfeld, D., Sauer, D., Schlager, H., Schnaiter, M.,
754 Schneider, J., Schulz, C., Spanu, A., Sperling, V. B., Voigt, C., Walser, A., Wang, J., Weinzierl, B.,
755 Wendisch, M. and Ziereis, H.: Aerosol characteristics and particle production in the upper
756 troposphere over the Amazon Basin, *Atmos. Chem. Phys.*, 18(2), 921–961,
757 doi:10.5194/acp-18-921-2018, 2018.

758 Arneth, A., Monson, R. K., Schurgers, G., Niinemets, Ü. and Palmer, P. I.: Why are estimates of
759 global terrestrial isoprene emissions so similar (and why is this not so for monoterpenes)?,
760 *Atmos. Chem. Phys.*, 8(16), 4605–4620, doi:10.5194/acp-8-4605-2008, 2008.

761 Berndt, T., Richters, S., Jokinen, T., Hyttinen, N., Kurtén, T., Otkjær, R. V., Kjaergaard, H. G.,
762 Stratmann, F., Herrmann, H., Sipilä, M., Kulmala, M. and Ehn, M.: Hydroxyl radical-induced
763 formation of highly oxidized organic compounds, *Nat. Commun.*, 7(May), 13677,

764 doi:10.1038/ncomms13677, 2016.

765 Berndt, T., Mentler, B., Scholz, W., Fischer, L., Herrmann, H., Kulmala, M. and Hansel, A.:
766 Accretion Product Formation from Ozonolysis and OH Radical Reaction of α -Pinene:
767 Mechanistic Insight and the Influence of Isoprene and Ethylene, *Environ. Sci. Technol.*,
768 doi:10.1021/acs.est.8b02210, 2018a.

769 Berndt, T., Scholz, W., Mentler, B., Fischer, L., Herrmann, H., Kulmala, M. and Hansel, A.:
770 Accretion Product Formation from Self- and Cross-Reactions of RO₂ Radicals in the
771 Atmosphere, *Angew. Chemie Int. Ed.*, 57(14), 3820–3824,
772 doi:https://doi.org/10.1002/anie.201710989, 2018b.

773 Bey, I., Jacob, D. J., Yantosca, R. M., Logan, J. A., Field, B. D., Fiore, A. M., Li, Q.-B., Liu, H.-Y.,
774 Mickley, L. J. and Schultz, M. G.: Global Modeling of Tropospheric Chemistry with Assimilated
775 Meteorology: Model Description and Evaluation, *J. Geophys. Res.*, 106, 73–95,
776 doi:10.1029/2001JD000807, 2001.

777 Bianchi, F., Trostl, J., Junninen, H., Frege, C., Henne, S., Hoyle, C. R., Molteni, U., Herrmann, E.,
778 Adamov, A., Bukowiecki, N., Chen, X., Duplissy, J., Gysel, M., Hutterli, M., Kangasluoma, J.,
779 Kontkanen, J., Kuerten, A., Manninen, H. E., Muench, S., Perakyla, O., Petaja, T., Rondo, L.,
780 Williamson, C., Weingartner, E., Curtius, J., Worsnop, D. R., Kulmala, M., Dommen, J. and
781 Baltensperger, U.: New particle formation in the free troposphere: A question of chemistry
782 and timing, *Science* (80-.), 352(6289), 1109–1112, doi:10.1126/science.aad5456, 2016.

783 Bianchi, F., Kurten, T., Riva, M., Mohr, C., Rissanen, M. P., Roldin, P., Berndt, T., Crouse, J. D.,
784 Wennberg, P. O., Mentel, T. F., Wildt, J., Junninen, H., Jokinen, T., Kulmala, M., Worsnop, D. R.,
785 Thornton, J. A., Donahue, N., Kjaergaard, H. G. and Ehn, M.: Highly Oxygenated Organic
786 Molecules (HOM) from Gas-Phase Autoxidation Involving Peroxy Radicals: A Key Contributor
787 to Atmospheric Aerosol, *Chem. Rev.*, 119(6), 3472–3509, doi:10.1021/acs.chemrev.8b00395,
788 2019.

789 Carlton, A. G., de Gouw, J., Jimenez, J. L., Ambrose, J. L., Attwood, A. R., Brown, S., Baker, K. R.,
790 Brock, C., Cohen, R. C., Edgerton, S., Farkas, C. M., Farmer, D., Goldstein, A. H., Gratz, L.,
791 Guenther, A., Hunt, S., Jaeglé, L., Jaffe, D. A., Mak, J., McClure, C., Nenes, A., Nguyen, T. K.,
792 Pierce, J. R., de Sa, S., Selin, N. E., Shah, V., Shaw, S., Shepson, P. B., Song, S., Stutz, J., Surratt,
793 J. D., Turpin, B. J., Warneke, C., Washenfelder, R. A., Wennberg, P. O. and Zhou, X.: Synthesis
794 of the Southeast Atmosphere Studies: Investigating Fundamental Atmospheric Chemistry
795 Questions, *Bull. Am. Meteorol. Soc.*, 99(3), 547–567, doi:10.1175/BAMS-D-16-0048.1, 2018.

796 DeCarlo, P. F., Kimmel, J. R., Trimborn, A., Northway, M. J., Jayne, J. T., Aiken, A. C., Gonin, M.,
797 Fuhrer, K., Horvath, T., Docherty, K. S., Worsnop, D. R. and Jimenez, J. L.: Field-Deployable,
798 High-Resolution, Time-of-Flight Aerosol Mass Spectrometer, *Anal. Chem.*, 78(24), 8281–8289,
799 doi:10.1021/ac061249n, 2006.

800 Ehn, M., Thornton, J. A., Kleist, E., Sipila, M., Junninen, H., Pullinen, I., Springer, M., Rubach, F.,
801 Tillmann, R., Lee, B., Lopez-Hilfiker, F., Andres, S., Acir, I.-H., Rissanen, M., Jokinen, T.,
802 Schobesberger, S., Kangasluoma, J., Kontkanen, J., Nieminen, T., Kurten, T., Nielsen, L. B.,
803 Jorgensen, S., Kjaergaard, H. G., Canagaratna, M., Dal Maso, M., Berndt, T., Petaja, T., Wahner,
804 A., Kerminen, V.-M., Kulmala, M., Worsnop, D. R., Wildt, J. J., Mentel, T. F., Maso, M. D.,
805 Berndt, T., Petaja, T., Wahner, A., Kerminen, V.-M., Kulmala, M., Worsnop, D. R., Wildt, J. J.
806 and Mentel, T. F.: A large source of low-volatility secondary organic aerosol, *Nature*,
807 506(7489), 476–479, doi:10.1038/nature13032, 2014.

808Fisher, J. A., Jacob, D. J., Travis, K. R., Kim, P. S., Marais, E. A., Chan Miller, C., Yu, K., Zhu, L.,
809 Yantosca, R. M., Sulprizio, M. P., Mao, J., Wennberg, P. O., Crouse, J. D., Teng, A. P., Nguyen,
810 T. B., St. Clair, J. M., Cohen, R. C., Romer, P., Nault, B. A., Wooldridge, P. J., Jimenez, J. L.,
811 Campuzano-Jost, P., Day, D. A., Hu, W., Shepson, P. B., Xiong, F., Blake, D. R., Goldstein, A. H.,
812 Misztal, P. K., Hanisco, T. F., Wolfe, G. M., Ryerson, T. B., Wisthaler, A. and Mikoviny, T.:
813 Organic nitrate chemistry and its implications for nitrogen budgets in an isoprene- and
814 monoterpene-rich atmosphere: constraints from aircraft (SEAC⁴SRS) and ground-based
815 (SOAS) observations in the Southeast US, *Atmos. Chem. Phys.*, 16(9), 5969–5991,
816 doi:10.5194/acp-16-5969-2016, 2016.

817Gelaro, R., McCarty, W., Suárez, M. J., Todling, R., Molod, A., Takacs, L., Randles, C. A., Darmenov,
818 A., Bosilovich, M. G., Reichle, R. and others: The modern-era retrospective analysis for
819 research and applications, version 2 (MERRA-2), *J. Clim.*, 30(14), 5419–5454, 2017.

820Guenther, A. B., Jiang, X., Heald, C. L., Sakulyanontvittaya, T., Duhl, T., Emmons, L. K. and Wang, X.:
821 The model of emissions of gases and aerosols from nature version 2.1 (MEGAN2.1): An
822 extended and updated framework for modeling biogenic emissions, *Geosci. Model Dev.*, 5(6),
823 1471–1492, doi:10.5194/gmd-5-1471-2012, 2012.

824Hallquist, M., Wenger, J. C., Baltensperger, U., Rudich, Y., Simpson, D., Claeys, M., Dommen, J.,
825 Donahue, N. M., George, C., Goldstein, A. H., Hamilton, J. F., Herrmann, H., Hoffmann, T.,
826 Iinuma, Y., Jang, M., Jenkin, M. E., Jimenez, J. L., Kiendler-Scharr, A., Maenhaut, W.,
827 McFiggans, G., Mentel, T. F., Monod, A., Prévôt, A. S. H., Seinfeld, J. H., Surratt, J. D.,
828 Szmigielski, R. and Wildt, J.: The formation, properties and impact of secondary organic
829 aerosol: current and emerging issues, *Atmos. Chem. Phys.*, 9(14), 5155–5236,
830 doi:10.5194/acp-9-5155-2009, 2009.

831Iyer, S., Rissanen, M. P., Valiev, R., Barua, S., Krechmer, J. E., Thornton, J., Ehn, M. and Kurtén, T.:
832 Molecular mechanism for rapid autoxidation in α -pinene ozonolysis, *Nat. Commun.*, 12(1),
833 878, doi:10.1038/s41467-021-21172-w, 2021.

834Jayne, J. T., Leard, D. C., Zhang, X., Davidovits, P., Smith, K. A., Kolb, C. E. and Worsnop, D. R.:
835 Development of an Aerosol Mass Spectrometer for Size and Composition Analysis of
836 Submicron Particles, *Aerosol Sci. Technol.*, 33(1–2), 49–70, doi:10.1080/027868200410840,
837 2000.

838Jimenez, J. L., Canagaratna, M. R., Donahue, N. M., Prevot, A. S. H., Zhang, Q., Kroll, J. H., DeCarlo,
839 P. F., Allan, J. D., Coe, H., Ng, N. L., Aiken, A. C., Docherty, K. S., Ulbrich, I. M., Grieshop, A. P.,
840 Robinson, A. L., Duplissy, J., Smith, J. D., Wilson, K. R., Lanz, V. A., Hueglin, C., Sun, Y. L., Tian,
841 J., Laaksonen, A., Raatikainen, T., Rautiainen, J., Vaattovaara, P., Ehn, M., Kulmala, M.,
842 Tomlinson, J. M., Collins, D. R., Cubison, M. J., Dunlea, J., Huffman, J. A., Onasch, T. B., Alfarra,
843 M. R., Williams, P. I., Bower, K., Kondo, Y., Schneider, J., Drewnick, F., Borrmann, S., Weimer, S.,
844 Demerjian, K., Salcedo, D., Cottrell, L., Griffin, R., Takami, A., Miyoshi, T., Hatakeyama, S.,
845 Shimono, A., Sun, J. Y., Zhang, Y. M., Dzepina, K., Kimmel, J. R., Sueper, D., Jayne, J. T.,
846 Herndon, S. C., Trimborn, A. M., Williams, L. R., Wood, E. C., Middlebrook, A. M., Kolb, C. E.,
847 Baltensperger, U. and Worsnop, D. R.: Evolution of Organic Aerosols in the Atmosphere,
848 *Science (80-.)*, 326(5959), 1525–1529, doi:10.1126/science.1180353, 2009.

849Jokinen, T., Berndt, T., Makkonen, R., Kerminen, V.-M., Junninen, H., Paasonen, P., Stratmann, F.,
850 Herrmann, H., Guenther, A. B., Worsnop, D. R., Kulmala, M., Ehn, M. and Sipilä, M.:
851 Production of extremely low volatile organic compounds from biogenic emissions: Measured

852 yields and atmospheric implications., *Proc. Natl. Acad. Sci. U. S. A.*, 112(23), 7123–8,
853 doi:10.1073/pnas.1423977112, 2015.

854 Keller, C. A., Long, M. S., Yantosca, R. M., Da Silva, A. M., Pawson, S. and Jacob, D. J.: HEMCO v1.0:
855 a versatile, ESMF-compliant component for calculating emissions in atmospheric models,
856 *Geosci. Model Dev.*, 7(4), 1409–1417, doi:10.5194/gmd-7-1409-2014, 2014.

857 Krapf, M., El Haddad, I., Bruns, E. A., Molteni, U., Daellenbach, K. R., Prévôt, A. S. H.,
858 Baltensperger, U., Dommen, J., Berndt, T., Richters, S., Kaethner, R., Voigtländer, J., Stratmann,
859 F., Sipilä, M., Kulmala, M., Herrmann, H., Crouse, J. D., Nielsen, L. B., Jørgensen, S.,
860 Kjaergaard, H. G., Wennberg, P. O., Ehn, M., Thornton, J. A., Kleist, E., Sipila, M., Junninen, H.,
861 Pullinen, I., Springer, M., Rubach, F., Tillmann, R., Lee, B., et Al., Jokinen, T., Berndt, T.,
862 Makkonen, R., Kerminen, V.-M., Junninen, H., Paasonen, P., Stratmann, F., Herrmann, H.,
863 Guenther, A. B., Worsnop, D. R., et Al., Jokinen, T., Sipilä, M., Richters, S., Kerminen, V.-M.,
864 Paasonen, P., Stratmann, F., Worsnop, D., Kulmala, M., Ehn, M., Herrmann, H., Berndt, T.,
865 Mentel, T. F., Springer, M., Ehn, M., Kleist, E., Pullinen, I., Kurtén, T., Rissanen, M., Wahner, A.,
866 Wildt, J., Richters, S., Herrmann, H., Berndt, T., Rissanen, M. P., Kurtén, T., Sipilä, M.,
867 Thornton, J. A., Kangasluoma, J., Sarnela, N., Junninen, H., Jørgensen, S., Schallhart, S., Kajos,
868 M. K., et Al., Heaton, K. J., Dreyfus, M. A., Wang, S., Johnston, M. V., Reinnig, M.-C., Warnke, J.,
869 Hoffmann, T., Ziemann, P. J., Aimanant, S., Ziemann, P. J., Docherty, K. S., Wu, W., Lim, Y. B.,
870 Ziemann, P. J., Mertes, P., Pfaffenberger, L., Dommen, J., Kalberer, M., Baltensperger, U.,
871 Nguyen, T. B., Bateman, A. P., Bones, D. L., et al.: Labile Peroxides in Secondary Organic
872 Aerosol, *Chem*, 1(4), 603–616, doi:10.1016/j.chempr.2016.09.007, 2016.

873 Kulmala, M., Petäjä, T., Ehn, M., Thornton, J., Sipilä, M., Worsnop, D. R. and Kerminen, V.-M.:
874 Chemistry of Atmospheric Nucleation: On the Recent Advances on Precursor
875 Characterization and Atmospheric Cluster Composition in Connection with Atmospheric New
876 Particle Formation, *Annu. Rev. Phys. Chem.*, 65(1),
877 doi:doi:10.1146/annurev-physchem-040412-110014, 2014.

878 Kurten, T., Rissanen, M. P., Mackeprang, K., Thornton, J. A., Hyttinen, N., Jørgensen, S., Ehn, M.,
879 Kjaergaard, H. G., Kurtén, T., Rissanen, M. P., Mackeprang, K., Thornton, J. A., Hyttinen, N.,
880 Jørgensen, S., Ehn, M. and Kjaergaard, H. G.: Computational Study of Hydrogen Shifts and
881 Ring-Opening Mechanisms in α -Pinene Ozonolysis Products, *J. Phys. Chem. A*, 119(46),
882 11366–11375, doi:10.1021/acs.jpca.5b08948, 2015.

883 Lee, B. H., Mohr, C., Lopez-Hilfiker, F. D., Lutz, A., Hallquist, M., Lee, L., Romer, P., Cohen, R. C.,
884 Iyer, S., Kurten, T., Hu, W., Day, D. A., Campuzano-Jost, P., Jimenez, J. L., Xu, L., Ng, N. L., Guo,
885 H., Weber, R. J., Wild, R. J., Brown, S. S., Koss, A., de Gouw, J., Olson, K., Goldstein, A. H., Seco,
886 R., Kim, S., McAvey, K., Shepson, P. B., Starn, T., Baumann, K., Edgerton, E. S., Liu, J., Shilling, J.
887 E., Miller, D. O., Brune, W., Schobesberger, S., D'Ambro, E. L., Thornton, J. A., Kurtén, T., Hu,
888 W., Day, D. A., Campuzano-Jost, P., Jimenez, J. L., Xu, L., Ng, N. L., Guo, H., Weber, R. J., Wild,
889 R. J., Brown, S. S., Koss, A., de Gouw, J., Olson, K., Goldstein, A. H., Seco, R., Kim, S., McAvey,
890 K., Shepson, P. B., Starn, T., Baumann, K., Edgerton, E. S., Liu, J., Shilling, J. E., Miller, D. O.,
891 Brune, W., Schobesberger, S., D'Ambro, E. L. and Thornton, J. A.: Highly
892 functionalized organic nitrates in the southeast United States: Contribution to secondary
893 organic aerosol and reactive nitrogen budgets, *Proc. Natl. Acad. Sci.*, 113(6), 1516–1521,
894 doi:10.1073/pnas.1508108113, 2016.

895 Lee, B. H., Lopez-Hilfiker, F. D., D'Ambro, E. L., Zhou, P., Boy, M., Petaja, T., Hao, L., Virtanen, A.

896 and Thornton, J. A.: Semi-volatile and highly oxygenated gaseous and particulate organic
897 compounds observed above a boreal forest canopy, *Atmos. Chem. Phys.*, 18(15), 11547–
898 11562, doi:10.5194/acp-18-11547-2018, 2018.

899 Lee, B. H., D'Ambro, E. L., Lopez-Hilfiker, F. D., Schobesberger, S., Mohr, C., Zawadowicz, M. A., Liu,
900 J., Shilling, J. E., Hu, W., Palm, B. B., Jimenez, J. L., Hao, L., Virtanen, A., Zhang, H., Goldstein,
901 A. H., Pye, H. O. T. and Thornton, J. A.: Resolving Ambient Organic Aerosol Formation and
902 Aging Pathways with Simultaneous Molecular Composition and Volatility Observations, *ACS*
903 *Earth Sp. Chem.*, 4(3), 391–402, doi:10.1021/acsearthspacechem.9b00302, 2020.

904 Liu, H., Jacob, D. J., Bey, I. and Yantosca, R. M.: Constraints from ²¹⁰Pb and ⁷Be on wet
905 deposition and transport in a global three-dimensional chemical tracer model driven by
906 assimilated meteorological fields, *J. Geophys. Res. Atmos.*, 106(D11), 12109–12128,
907 doi:https://doi.org/10.1029/2000JD900839, 2001.

908 Lopez-Hilfiker, F. D., Mohr, C., Ehn, M., Rubach, F., Kleist, E., Wildt, J., Mentel, T. F., Lutz, A.,
909 Hallquist, M., Worsnop, D. and Thornton, J. A.: A novel method for online analysis of gas and
910 particle composition: description and evaluation of a Filter Inlet for Gases and AEROSols
911 (FIGAERO), *J. Geophys. Res. Atmos.*, 119(4), 983–1001, doi:10.5194/amt-7-983-2014, 2014.

912 Lopez-Hilfiker, F. D., Mohr, C., D'Ambro, E. L., Lutz, A., Riedel, T. P., Gaston, C. J., Iyer, S., Zhang, Z.,
913 Gold, A., Surratt, J. D., Lee, B. H., Kurten, T., Hu, W. W., Jimenez, J., Hallquist, M. and Thornton,
914 J. A.: Molecular Composition and Volatility of Organic Aerosol in the Southeastern U.S.:
915 Implications for IEPOX Derived SOA, *Environ. Sci. Technol.*, 50(5), 2200–2209,
916 doi:10.1021/acs.est.5b04769, 2016.

917 Mao, J., Jacob, D. J., Evans, M. J., Olson, J. R., Ren, X., Brune, W. H., St. Clair, J. M., Crouse, J. D.,
918 Spencer, K. M., Beaver, M. R., Wennberg, P. O., Cubison, M. J., Jimenez, J. L., Fried, A.,
919 Weibring, P., Walega, J. G., Hall, S. R., Weinheimer, A. J., Cohen, R. C., Chen, G., Crawford, J.
920 H., McNaughton, C., Clarke, A. D., Jaeglé, L., Fisher, J. A., Yantosca, R. M., Le Sager, P. and
921 Carouge, C.: Chemistry of hydrogen oxide radicals (HO_x) in the Arctic troposphere in spring,
922 *Atmos. Chem. Phys.*, 10(13), 5823–5838, doi:10.5194/acp-10-5823-2010, 2010.

923 Mao, J., Paulot, F., Jacob, D. J., Cohen, R. C., Crouse, J. D., Wennberg, P. O., Keller, C. A., Hudman,
924 R. C., Barkley, M. P. and Horowitz, L. W.: Ozone and organic nitrates over the eastern United
925 States: Sensitivity to isoprene chemistry, *J. Geophys. Res. Atmos.*, 118(19), 11256–11268,
926 doi:10.1002/jgrd.50817, 2013.

927 Martin, S. T., Artaxo, P., Machado, L. A. T., Manzi, A. O., Souza, R. A. F., Schumacher, C., Wang, J.,
928 Andreae, M. O., Barbosa, H. M. J., Fan, J., Fisch, G., Goldstein, A. H., Guenther, A., Jimenez, J.
929 L., Pöschl, U., Silva Dias, M. A., Smith, J. N. and Wendisch, M.: Introduction: Observations and
930 Modeling of the Green Ocean Amazon (GoAmazon2014/5), *Atmos. Chem. Phys.*, 16(8),
931 4785–4797, doi:10.5194/acp-16-4785-2016, 2016.

932 Massoli, P., Stark, H., Canagaratna, M. R., Krechmer, J. E., Xu, L., Ng, N. L., Mauldin, R. L., Yan, C.,
933 Kimmel, J., Misztal, P. K., Jimenez, J. L., Jayne, J. T. and Worsnop, D. R.: Ambient
934 Measurements of Highly Oxidized Gas-Phase Molecules during the Southern Oxidant and
935 Aerosol Study (SOAS) 2013, *ACS Earth Sp. Chem.*, 2(7), 653–672,
936 doi:10.1021/acsearthspacechem.8b00028, 2018.

937 McDonald, B. C., de Gouw, J. A., Gilman, J. B., Jathar, S. H., Akherati, A., Cappa, C. D., Jimenez, J.
938 L., Lee-Taylor, J., Hayes, P. L., McKeen, S. A., Cui, Y. Y., Kim, S.-W., Gentner, D. R.,
939 Isaacman-VanWertz, G., Goldstein, A. H., Harley, R. A., Frost, G. J., Roberts, J. M., Ryerson, T.

940 B. and Trainer, M.: Volatile chemical products emerging as largest petrochemical source of
941 urban organic emissions, *Science* (80-.), 359(6377), 760–764, doi:10.1126/science.aaq0524,
942 2018.

943McFiggans, G., Mentel, T. F., Wildt, J., Pullinen, I., Kang, S., Kleist, E., Schmitt, S., Springer, M.,
944 Tillmann, R., Wu, C., Zhao, D., Hallquist, M., Faxon, C., Le Breton, M., Hallquist, A. M.,
945 Simpson, D., Bergstroem, R., Jenkin, M. E., Ehn, M., Thornton, J. A., Alfarra, M. R., Bannan, T.
946 J., Percival, C. J., Priestley, M., Topping, D. and Kiendler-Scharr, A.: Secondary organic aerosol
947 reduced by mixture of atmospheric vapours, *Nature*, 565(7741), 587–593,
948 doi:10.1038/s41586-018-0871-y, 2019.

949Mentel, T. F., Springer, M., Ehn, M., Kleist, E., Pullinen, I., Kurtén, T., Rissanen, M., Wahner, A. and
950 Wildt, J.: Formation of highly oxidized multifunctional compounds: autoxidation of peroxy
951 radicals formed in the ozonolysis of alkenes – deduced from structure–product relationships,
952 *Atmos. Chem. Phys.*, 15(12), 6745–6765, doi:10.5194/acp-15-6745-2015, 2015.

953Messina, P., Lathière, J., Sindelarova, K., Vuichard, N., Granier, C., Ghattas, J., Cozic, A. and
954 Hauglustaine, D. A.: Global biogenic volatile organic compound emissions in the ORCHIDEE
955 and MEGAN models and sensitivity to key parameters, *Atmos. Chem. Phys.*, 16(22), 14169–
956 14202, doi:10.5194/acp-16-14169-2016, 2016.

957Orlando, J. J., Tyndall, G. S. and Wallington, T. J.: The Atmospheric Chemistry of Alkoxy Radicals,
958 *Chem. Rev.*, 103(12), 4657–4690, doi:10.1021/cr020527p, 2003.

959Öström, E., Putian, Z., Schurgers, G., Mishurov, M., Kivekäs, N., Lihavainen, H., Ehn, M., Rissanen,
960 M. P., Kurtén, T., Boy, M., Swietlicki, E. and Roldin, P.: Modeling the role of highly oxidized
961 multifunctional organic molecules for the growth of new particles over the boreal forest
962 region, *Atmos. Chem. Phys.*, 17(14), 8887–8901, doi:10.5194/acp-17-8887-2017, 2017.

963Palen, E. J., Allen, D. T., Pandis, S. N., Paulson, S. E., Seinfeld, J. H. and Flagan, R. C.: Fourier
964 transform infrared analysis of aerosol formed in the photo-oxidation of isoprene and
965 β -pinene, *Atmos. Environ. Part A. Gen. Top.*, 26(7), 1239–1251,
966 doi:https://doi.org/10.1016/0960-1686(92)90385-X, 1992.

967Pandis, S. N., Harley, R. A., Cass, G. R. and Seinfeld, J. H.: Secondary organic aerosol formation
968 and transport, *Atmos. Environ. Part A. Gen. Top.*, 26(13), 2269–2282,
969 doi:https://doi.org/10.1016/0960-1686(92)90358-R, 1992.

970Petaja, T., O’Connor, E. J., Moiseev, D., Sinclair, V. A. V. A., Manninen, A. J. A. J., Vaananen, R., von
971 Lerber, A., Thornton, J. A., Nicocoll, K., Petersen, W., Chandrasekar, V., Smith, J. N., Winkler,
972 P. M., Krueger, O., Hakola, H., Timonen, H., Brus, D., Laurila, T., Asmi, E., Riekkola, M.-L.,
973 Mona, L., Massoli, P., Engelmann, R., Kompppula, M., Wang, J., Kuang, C., Baeck, J., Virtanen,
974 A., Levula, J., Ritsche, M., Hickmon, N., Petäjä, T., O’Connor, E. J., Moiseev, D., Sinclair, V. A. V.
975 A., Manninen, A. J. A. J., Väänänen, R., von Lerber, A., Thornton, J. A., Nicoll, K., Petersen, W.,
976 Chandrasekar, V., Smith, J. N., Winkler, P. M., Krüger, O., Hakola, H., Timonen, H., Brus, D.,
977 Laurila, T., Asmi, E., Riekkola, M.-L., Mona, L., Massoli, P., Engelmann, R., Komppula, M.,
978 Wang, J., Kuang, C., Bäck, J., Virtanen, A., Levula, J., Ritsche, M. and Hickmon, N.: BAECC: A
979 Field Campaign to Elucidate the Impact of Biogenic Aerosols on Clouds and Climate, *Bull. Am.*
980 *Meteorol. Soc.*, 97(10), 1909–1928, doi:10.1175/BAMS-D-14-00199.1, 2016.

981Pospisilova, V., Lopez-Hilfiker, F. D., Bell, D. M., El Haddad, I., Mohr, C., Huang, W., Heikkinen, L.,
982 Xiao, M., Dommen, J., Prevot, A. S. H., Baltensperger, U. and Slowik, J. G.: On the fate of
983 oxygenated organic molecules in atmospheric aerosol particles, *Sci. Adv.*, 6(11),

984 doi:10.1126/sciadv.aax8922, 2020.

985 [Pullinen, I., Schmitt, S., Kang, S., Sarrafzadeh, M., Schlag, P., Andres, S., Kleist, E., Mentel, T. F.,](#)
986 [Rohrer, F., Springer, M., Tillmann, R., Wildt, J., Wu, C., Zhao, D., Wahner, A., and](#)
987 [Kiendler-Scharr, A.: Impact of NO_x on secondary organic aerosol \(SOA\) formation from](#)
988 [α-pinene and β-pinene photooxidation: the role of highly oxygenated organic nitrates, *Atmos.*](#)
989 [Chem. Phys., 20, 10125–10147, <https://doi.org/10.5194/acp-20-10125-2020>, 2020](#)

990 Richters, S., Herrmann, H. and Berndt, T.: Highly Oxidized RO₂ Radicals and Consecutive Products
991 from the Ozonolysis of Three Sesquiterpenes, *Environ. Sci. & Technol.*, 50(5), 2354–2362,
992 doi:10.1021/acs.est.5b05321, 2016.

993 [Roldin, P., Ehn, M., Kurtén, T., Olenius, T., Rissanen, M. P., Sarnela, N., Elm, J., Rantala, P., Hao, L.,](#)
994 [Hyttinen, N., Heikkinen, L., Worsnop, D. R., Pichelstorfer, L., Xavier, C., Clusius, P., Öström, E.,](#)
995 [Petäjä, T., Kulmala, M., Vehkamäki, H., Virtanen, A., Riipinen, I. and Boy, M.: The role of](#)
996 [highly oxygenated organic molecules in the Boreal aerosol-cloud-climate system, *Nat.*](#)
997 [Commun., 10\(1\), 4370, doi:10.1038/s41467-019-12338-8, 2019.](#)

998 de Sa, S. S., Palm, B. B., Campuzano-Jost, P., Day, D. A., Hu, W., Isaacman-VanWertz, G., Yee, L. D.,
999 Brito, J., Carbone, S., Ribeiro, I. O., Cirino, G. G., Liu, Y., Thalman, R., Sedlacek, A., Funk, A.,
1000 Schumacher, C., Shilling, J. E., Schneider, J., Artaxo, P., Goldstein, A. H., Souza, R. A. F., Wang,
1001 J., McKinney, K. A., Barbosa, H., Alexander, M. L., Jimenez, J. L. and Martin, S. T.: Urban
1002 influence on the concentration and composition of submicron particulate matter in central
1003 Amazonia, *Atmos. Chem. Phys.*, 18(16), 12185–12206, doi:10.5194/acp-18-12185-2018,
1004 2018.

1005 Travis, K. R., Jacob, D. J., Fisher, J. A., Kim, P. S., Marais, E. A., Zhu, L., Yu, K., Miller, C. C., Yantosca,
1006 R. M., Sulprizio, M. P., Thompson, A. M., Wennberg, P. O., Crouse, J. D., St Clair, J. M., Cohen,
1007 R. C., Laughner, J. L., Dibb, J. E., Hall, S. R., Ullmann, K., Wolfe, G. M., Pollack, I. B., Peischl, J.,
1008 Neuman, J. A. and Zhou, X.: Why do models overestimate surface ozone in the Southeast
1009 United States?, *Atmos. Chem. Phys.*, 16(21), 13561–13577, doi:10.5194/acp-16-13561-2016,
1010 2016.

1011 Wang, J., Krejci, R., Giangrandel, S., Kuang, C., Barbosa, H. M. J., Brito, J., Carbone, S., Chi, X.,
1012 Comstock, J., Ditas, F., Lavric, J., Manninen, H. E., Mei, F., Moran-Zuloaga, D., Pöhlker, C.,
1013 Pöhlker, M. L., Saturno, J., Schmid, B., Souza, R. A. F., Springston, S. R., Tomlinson, J. M., Toto,
1014 T., Walter, D., Wimmer, D., Smith, J. N., Kulmala, M., Machado, L. A. T., Artaxo, P., Andreae, M.
1015 O., Petaja, T. and Martin, S. T.: Amazon boundary layer aerosol concentration sustained by
1016 vertical transport during rainfall, *Nature*, 539(7629), 416–419, doi:10.1038/nature19819,
1017 2016.

1018 Weber, J., Archer-Nicholls, S., Griffiths, P., Berndt, T., Jenkin, M., Gordon, H., Knote, C. and
1019 Archibald, A. T.: CRI-HOM: A novel chemical mechanism for simulating highly oxygenated
1020 organic molecules (HOMs) in global chemistry--aerosol--climate models, *Atmos. Chem. Phys.*,
1021 20(18), 10889–10910, doi:10.5194/acp-20-10889-2020, 2020.

1022 Wesely, M. L.: Parameterization of surface resistances to gaseous dry deposition in regional-scale
1023 numerical models, *Atmos. Environ.*, 23(6), 1293–1304,
1024 doi:[https://doi.org/10.1016/0004-6981\(89\)90153-4](https://doi.org/10.1016/0004-6981(89)90153-4), 1989.

1025 Xu, L., Pye, H. O. T., He, J., Chen, Y., Murphy, B. N. and Ng, N. L.: Experimental and model
1026 estimates of the contributions from biogenic monoterpenes and sesquiterpenes to
1027 secondary organic aerosol in the southeastern United States, *Atmos. Chem. Phys.*, 18(17),

1028 12613–12637, doi:10.5194/acp-18-12613-2018, 2018.

1029 Xu, L., Møller, K. H., Crouse, J. D., Otkjær, R. V., Kjaergaard, H. G. and Wennberg, P. O.:
1030 Unimolecular reactions of peroxy radicals formed in the oxidation of α -Pinene and β -Pinene
1031 by hydroxyl radicals, *J. Phys. Chem. A*, doi:10.1021/acs.jpca.8b11726, 2019.

1032 Zawadowicz, M. A., Lee, B. H., Shrivastava, M., Zelenyuk, A., Zaveri, R. A., Flynn, C., Thornton, J. A.
1033 and Shilling, J. E.: Photolysis Controls Atmospheric Budgets of Biogenic Secondary Organic
1034 Aerosol, *Environ. Sci. & Technol.*, 54(7), 3861–3870, doi:10.1021/acs.est.9b07051, 2020.

1035 Zhang, H., Yee, L. D., Lee, B. H., Curtis, M. P., Worton, D. R., Isaacman-VanWertz, G., Offenberg, J.
1036 H., Lewandowski, M., Kleindienst, T. E., Beaver, M. R., Holder, A. L., Lonneman, W. A.,
1037 Docherty, K. S., Jaoui, M., Pye, H. O. T., Hu, W., Day, D. A., Campuzano-Jost, P., Jimenez, J. L.,
1038 Guo, H., Weber, R. J., de Gouw, J., Koss, A. R., Edgerton, E. S., Brune, W., Mohr, C.,
1039 Lopez-Hilfiker, F. D., Lutz, A., Kreisberg, N. M., Spielman, S. R., Hering, S. V., Wilson, K. R.,
1040 Thornton, J. A. and Goldstein, A. H.: Monoterpenes are the largest source of summertime
1041 organic aerosol in the southeastern United States, *Proc. Natl. Acad. Sci. U. S. A.*, 115(9),
1042 2038–2043, doi:10.1073/pnas.1717513115, 2018.

1043 Zhang, L., Gong, S., Padro, J. and Barrie, L.: A size-segregated particle dry deposition scheme for
1044 an atmospheric aerosol module, *Atmos. Environ.*, 35(3), 549–560,
1045 doi:https://doi.org/10.1016/S1352-2310(00)00326-5, 2001.

1046 Zhang, S.-H., Shaw, M., Seinfeld, J. H. and Flagan, R. C.: Photochemical aerosol formation from
1047 α -pinene- and β -pinene, *J. Geophys. Res. Atmos.*, 97(D18), 20717–20729,
1048 doi:https://doi.org/10.1029/92JD02156, 1992.

1049 Zhao, B., Shrivastava, M., Donahue, N. M., Gordon, H., Schervish, M., Shilling, J. E., Zaveri, R. A.,
1050 Wang, J., Andreae, M. O., Zhao, C., Gaudet, B., Liu, Y., Fan, J. and Fast, J. D.: High
1051 concentration of ultrafine particles in the Amazon free troposphere produced by organic new
1052 particle formation, *Proc. Natl. Acad. Sci.*, 117(41), 25344–25351,
1053 doi:10.1073/pnas.2006716117, 2020.

1054 Zhao, Y., Thornton, J. A. and Pye, H. O. T.: Quantitative constraints on autoxidation and dimer
1055 formation from direct probing of monoterpene-derived peroxy radical chemistry, *Proc. Natl.*
1056 *Acad. Sci. U. S. A.*, 115(48), 12142–12147, doi:10.1073/pnas.1812147115, 2018.

1057 [Zhu, J., Penner, J.E., Yu, F., Sillman, S., Andreae, M. O., Coe, H. Decrease in radiative forcing by
1058 organic aerosol nucleation, climate, and land use change, *Nat. Commun.*, **10**, 423 \(2019\).
1059 <https://doi.org/10.1038/s41467-019-08407-7>](https://doi.org/10.1038/s41467-019-08407-7)

1060

Formatted: Font: Not Italic

Formatted: Font: Not Italic